B V+ in the Standard Model from light-cone sum rules

TUM-HEP-957/14
CP3-Origins-2015-010 DNRF90
DIAS-2015-10

$B \to V\ell^+\ell^-$ in the Standard Model from Light-Cone Sum Rules

Aoife Bharucha[a,b], David M. Straub[c], and Roman Zwicky[d]

[a] Physik Department T31, Technische Universität München, James-Franck-Str. 1, 85748 Garching, Germany

[b] CNRS, Aix Marseille U., U. de Toulon, CPT, UMR 7332, F-13288, Marseille, France

[c] Excellence Cluster Universe, Technische Universität München, Boltzmannstr. 2, 85748 Garching, Germany

[d] Higgs Centre for Theoretical Physics, School of Physics and Astronomy, University of Edinburgh, Edinburgh EH9 3JZ, Scotland

E-Mail: aoife.bharucha@cpt.univ-mrs.fr, david.straub@tum.de, roman.zwicky@ed.ac.uk.

We present $B_q \to \rho$, $B_q \to \omega$, $B_q \to K^*$, $B_s \to K^*$ and $B_s \to \phi$ form factors from light-cone sum rules using updated hadronic input parameters. It is argued that the, generally valid, equations of motion constrain the uncertainty of tensor-to-vector form factor ratios. This improves the prediction of zeros of helicity amplitudes which is of major importance for $B \to K^*\ell\ell$ angular observables. We provide easy-to-use fits to the LCSR results, including the full error correlation matrix, in all modes at low q^2 as well as combined fits to LCSR and lattice results covering the entire kinematic range for $B_q \to K^*$, $B_s \to K^*$ and $B_s \to \phi$. The error correlation matrix avoids the problem of overestimating the uncertainty in phenomenological applications. Using the new form factors and recent computations of non-factorisable contributions we provide Standard Model predictions for $B \to K^*\gamma$ as well as $B \to K^*\ell^+\ell^-$ and $B_s \to \phi\mu^+\mu^-$ at low dilepton invariant mass. Employing our $B \to (\rho,\omega)$ form factor results we extract the CKM element $|V_{\rm ub}|$ from the semileptonic decays $B \to (\rho,\omega)\ell\nu$, and find good agreement with other exclusive determinations.

Contents

1. Introduction

Exclusive semi-leptonic B decays are important tools to test the Standard Model (SM) and to look for new physics. Among these processes, the decays $B \to K^*(\to K\pi)\mu^+\mu^-$ and $B_s \to \phi(\to KK)\mu^+\mu^-$ are of particular relevance as their angular distributions give access to a host of observables that are sensitive to new physics. Predicting these observables, either within the SM or beyond, requires the knowledge of the form factors – in the case of $B \to V$ transitions, these are 7 functions of the dilepton invariant mass squared q^2. In the low q^2 region, where the vector meson is energetic, the form factors can be computed using the method of sum rules on the light cone (LCSR) whereas at high q^2 the form factors can be computed using lattice QCD.

In this work we present an update of the form factor computation in [1], for the modes $B_q \to \rho$, $B_q \to \omega$, $B_q \to K^*$, $B_s \to K^*$ and $B_s \to \phi$ (with $q = u, d$), using current hadronic input and a concise discussion of the role of *the equation of motion* in correlating the vector and tensor form factors. The form factors are fitted to the z-expansion parameterisation in the helicity basis, *retaining all correlations* among the expansion coefficients. This information is made publicly available as ancillary files on the arXiv web pages in a form which is easy to use for phenomenology.

Crucially the correlation of the uncertainties avoids overestimating uncertainties in observables. A particularly important example are the angular observables in $B \to K^*\mu^+\mu^-$-type decays since they are sensitive to ratios of form factors and zeros of helicity amplitudes. For the latter two, the uncertainty is considerably reduced when taking correlation into account.

We argue, extending the work in ref. [2], that the use of the equation of motion enforces the correlation of the non-parametric, sum rule specific, input parameters. This can be seen as an application of the large energy limit (LEL) ideas [3] to the sum rules on the light-cone. It is in giving numerical predictions and not relying on the heavy quark limit that the LCSR computations go beyond the LEL ideas [3]; including the use of the factorisable hard α_s-corrections [4]. The LCSR therefore give corrections to the LEL [3] and soft-collinear effective theory (SCET) [4] relations. Going beyond the SCET framework, of two soft form factors and hard α_s-correction in the heavy quark limit, involves using the numerical predictions from LCSR, e.g. [5]. Going beyond the SCET framework has become increasingly important since observables designed to minimise the impact of the soft form factors [6] are, of course, sensitive to $1/m_b$-corrections.

We perform *combined fits* of the form factors to the LCSR at low q^2 and the above mentioned lattice computation at high q^2. This serves to test the consistency of the two complementary methods and to provide form factor sets valid over the entire kinematical region. We extract the CKM element $|V_{\rm ub}|$ from $B \to (\omega, \rho)\ell\nu$ BaBar- and Belle-data using the $B \to (\omega, \rho)$ form factor predictions of this paper. This can either be viewed as an extraction of $|V_{\rm ub}|$ or as a check of the normalisation of the form factor when compared to global fits or $B \to \pi\ell\nu$ extractions. In addition to the form factors, the calculation of $B \to V\ell^+\ell^-$ observables involves *non-factorisable contributions* from the weak hadronic Hamiltonian. Some of these contributions have been recently computed within LCSR. Including all of these ingredients, we present SM predictions for the branching ratios and angular observables of $B \to K^*\mu^+\mu^-$ and $B_s \to \phi\mu^+\mu^-$. We also compare the prediction for the branching ratio of $B \to K^*\gamma$, that has been measured precisely at the B factories, to the data.

The paper is organised as follows. In section 2 we present and discuss the seven $B \to V$ form factors within the LCSR context, discussing the implication of the equation of motion,

finite width effects, input parameters and the interpolating fits to the lattice data. In section 3 phenomenological aspects of $B \to K^*\mu\mu$, $B \to K^*\gamma$, $B_s \to \phi\mu\mu$, $B \to K^*\mu\mu$ versus $B_s \to \phi\mu\mu$ and the determination of $|V_{\rm ub}|$ from $B \to (\rho,\omega)\ell\nu$ are discussed: see subsections 3.1, 3.2, 3.3, 3.4 and 3.5 respectively. Conclusions figure in section 4. Appendix A assembles aspects of the equation of motion, explicit tree level results, scheme dependence and remarks on the Borel parameters. Conversion between bases, further plots and fit coefficients are given in appendixes B, C, and D respectively. The effect of the sizeable B_s-lifetime is worked out in E.

2. $B \to V$ form factors from light-cone sum rules

The short distance matrix elements, relevant for the dimension six effective Hamiltonian, are parameterised by seven form factors,

$$\begin{aligned}\langle K^*(p,\eta)|\bar{s}\gamma^\mu(1\mp\gamma_5)b|\bar{B}(p_B)\rangle &= P_1^\mu\,\mathcal{V}_1(q^2) \pm P_2^\mu\,\mathcal{V}_2(q^2) \pm P_3^\mu\,\mathcal{V}_3(q^2) \pm P_P^\mu\mathcal{V}_P(q^2)\,,\\ \langle K^*(p,\eta)|\bar{s}iq_\nu\sigma^{\mu\nu}(1\pm\gamma_5)b|\bar{B}(p_B)\rangle &= P_1^\mu T_1(q^2) \pm P_2^\mu T_2(q^2) \pm P_3^\mu T_3(q^2)\,,\end{aligned} \tag{1}$$

where the Lorentz structures P_i^μ are defined as in [7]

$$\begin{aligned} P_P^\mu &= i(\eta^*\cdot q)q^\mu\,, & P_1^\mu &= 2\epsilon^\mu{}_{\alpha\beta\gamma}\eta^{*\alpha}p^\beta q^\gamma\,,\\ P_2^\mu &= i\{(m_B^2-m_{K^*}^2)\eta^{*\mu}-(\eta^*\cdot q)(p+p_B)^\mu\}\,, & P_3^\mu &= i(\eta^*\cdot q)\{q^\mu-\frac{q^2}{m_B^2-m_{K^*}^2}(p+p_B)^\mu\}\,,\end{aligned} \tag{2}$$

with the $\epsilon_{0123}=+1$ convention for the Levi-Civita tensor. The relation $T_1(0)=T_2(0)$ holds algebraically. The parameterisation (1) makes the correspondence between vector and tensor form factors explicit. The correspondence of the $\mathcal{V}_{P,1,2,3}$ to the more traditional form factors $A_{0,1,2,3}$ and V is as follows

$$\begin{aligned}\mathcal{V}_P(q^2) &= \frac{-2m_{K^*}}{q^2}A_0(q^2)\,, \quad \mathcal{V}_1(q^2) = \frac{-V(q^2)}{m_B+m_{K^*}}\,, \quad \mathcal{V}_2(q^2) = \frac{-A_1(q^2)}{m_B-m_{K^*}}\,,\\ \mathcal{V}_3(q^2) &= \big(\frac{m_B+m_{K^*}}{q^2}A_1(q^2) - \frac{m_B-m_{K^*}}{q^2}A_2(q^2)\big) \equiv \frac{2m_{K^*}}{q^2}A_3(q^2)\,.\end{aligned} \tag{3}$$

The relation $A_3(0)=A_0(0)$ assures finite matrix elements at $q^2=0$. The last relation in (3) indicates that one form factor out of $A_{1,2,3}$ is redundant.[1] The pseudoscalar matrix element is related to A_0 through the axial Ward Identity:

$$\langle K^*(p,\eta)|\bar{s}\gamma_5 b|\bar{B}(p_B)\rangle = \left(\frac{P_P\cdot q}{m_s+m_b}\right)\mathcal{V}_P(q^2) = \left(\frac{2m_{K^*}(\eta^*\cdot q)}{i(m_s+m_b)}\right)A_0(q^2)\,. \tag{4}$$

The projection on the helicity basis, using the Jacob-Wick polarisation convention, is given in appendix B. In the next section we briefly discuss the use of the method of LCSR before investigating the implications of the equation of motion (Ward Identities) on certain sum rule specific parameters.

[1] From the viewpoint of the projections the traditional nomenclature is unfortunate. It would have been better not to have A_2 at all and use the notation $A_1 \to A_2$.

2.1. Calculation of the form factors in light-cone sum rules

Light-cone sum rules (similar to QCD sum rules [8, 9]) for the form factors are derived by considering the correlator of the time-ordered product of two quark currents evaluated between the final state on-shell meson (in this case V) and the vacuum [10, 11]. On expanding this correlator about the light-cone, one obtains a series of perturbatively calculable hard scattering kernels convoluted with non-perturbative, universal light-cone distribution amplitudes, ordered by increasing twist (dimension minus spin) Reasonable convergence of the LC-expansion is formally and by experience limited up to $q^2 \simeq O(m_b \Lambda_{\rm QCD}) \simeq 14\,{\rm GeV}^2$. In the hadronic picture the correlator is expressed as the sum over excited states, the dominant state being the B-meson, and this is followed by the continuum. Assuming quark-hadron duality above a certain continuum threshold s_0 [8,9], an approximation referred to as semi-global quark-hadron duality assumption, one arrives at an expression for the lowest lying hadronic parameter in terms of an expression of partonic QCD and s_0. A Borel transformation which improves both the hadron and the parton evaluation leads to a numerical improvement of the procedure.

Light-cone sum rules results, with light-meson distribution amplitude (DA), for all seven form factors have previously been computed up to twist-4 at tree level and twist-2 $\mathcal{O}(\alpha_s)$ [12] as well as twist-3 $\mathcal{O}(\alpha_s)$ [1]. In this paper we make use of the results in [1]. An alternatively the form factors can be determined using B-meson DA and an interpolating current for the B-meson. This program has been pursued at the tree level approximation in [13].

2.2. Equation of motion and form factors

In this section we reiterate the use of the equation of motion (eom) [2]. As discussed in [2] this is of importance for the reduction of the uncertainty in the tensor-to-vector form factor ratio. Below we shall give more details and strengthen the argument. The following eom

$$i\partial^\nu(\bar s i\sigma_{\mu\nu}(\gamma_5)b) = -(m_s \pm m_b)\bar s\gamma_\mu(\gamma_5)b + i\partial_\mu(\bar s(\gamma_5)b) - 2\bar s i\overleftarrow{D}_\mu\,(\gamma_5)b\,, \tag{5}$$

are valid on physical states.

Equations of the form (5) are sometimes referred to as Ward identities; e.g. eq. (4). In particular, evaluated on $\langle V|..|B\rangle$ eq. (5) yields

$$T_1(q^2) + (m_b + m_s)\mathcal{V}_1(q^2) + \mathcal{D}_1(q^2) = 0\,, \tag{6}$$
$$T_2(q^2) + (m_b - m_s)\mathcal{V}_2(q^2) + \mathcal{D}_2(q^2) = 0\,, \tag{7}$$
$$T_3(q^2) + (m_b - m_s)\mathcal{V}_3(q^2) + \mathcal{D}_3(q^2) = 0\,, \tag{8}$$
$$(m_b - m_s)\mathcal{V}_P(q^2) + \left(\mathcal{D}_P(q^2) - \frac{q^2}{m_b + m_s}\mathcal{V}_P(q^2)\right) = 0\,. \tag{9}$$

One of the above four equations correponds to each of the directions (2) [2, 14], where $\mathcal{D}_\iota$ are defined

$$\langle K^*(p,\eta)|\bar s(2i\overleftarrow{D})^\mu(1\pm\gamma_5)b|\bar B(p_B)\rangle = P_1^\mu\,\mathcal{D}_1(q^2) \pm P_2^\mu\,\mathcal{D}_2(q^2) \pm P_3^\mu\,\mathcal{D}_3(q^2) \pm P_P^\mu\mathcal{D}_P(q^2)\,, \tag{10}$$

in complete analogy with (1). Note that the $i\partial_\mu(\bar s(\gamma_5)b)$ operator only contributes to $P_P^\mu \sim q^\mu$, since the total derivative is replaced by the momentum transfer q^μ. In eq. (9) we have included this contribution into round brackets with the other derivative form factor. Before discussing the eqs. (6)-(9) in various limits we wish to stress that the equation are completely general and have to be obeyed by any form factor determination.

The Isgur-Wise relations [15] at low recoil follow from the fact that it can be argued, using heavy quark effective theory, that the $\mathcal{D}_\iota$ are suppressed by $(\Lambda_{\rm QCD}/m_b)$ with respect to the vector and tensor form factors [14]. This raises the question of whether there are combinations of $\mathcal{D}_\iota$'s which are small at large recoil. eqs. (6,7) are direct candidates but eqs. (8,9) require some thought because of the common direction q_μ. In fact in eqs. (8,9) the poles in q^2 cancel between the form factor $\mathcal{V}_{3,P}$ and $\mathcal{D}_{3,P}$ and hence $\mathcal{D}_{3,P}$ are not individually small. Since the form factor $\langle K^*|\bar{s}\gamma_\mu\gamma_5 b|\bar{B}\rangle$ has no singularity, adding eqs. (8,9) yields a combination for which the derivative form factor are potentially small. We define the following ratios

$$\begin{aligned}
r_\perp(q^2) &= -\frac{(m_b+m_s)\mathcal{V}_1(q^2)}{T_1(q^2)}\,,\\
r_\parallel(q^2) &= -\frac{(m_b-m_s)\mathcal{V}_2(q^2)}{T_2(q^2)}\,,\\
r_{0+t}(q^2) &= -\frac{(m_b-m_s)(\mathcal{V}_2(q^2)-c_{23}(q^2)(\mathcal{V}_3(q^2)+\mathcal{V}_P(q^2)))}{T_2(q^2)-c_{23}(q^2)T_3(q^2)}\\
&= -\frac{(m_b-m_s)(\mathcal{V}_0(q^2)-c_{23}\mathcal{V}_P(q^2))}{T_0(q^2)}\,,
\end{aligned} \tag{11}$$

with $c_{23}(q^2)$ being a kinematic function defined in eq. (B.3). The deviations of these quantities from one measure the relative size of the derivative form factors with respect to vector and tensor form factors. For example $r_\perp = 1 + \mathcal{D}_1(q^2)/T_1(q^2)$. In fig. 1 we show plots of these quantities from $0 < q^2 < 14\,\text{GeV}^2$. The quantities $r_{\perp,\parallel}$ and, somewhat less, r_{0+t} are found to be very close to unity over this range. The basic idea is that of the $\mathcal{D}_i$ are considered as regular form factors with controlled uncertainty then the ratios r_i can never differ from one by a significant amount, as revealed by the relatively narrow error bands.

Let us discuss the regularity of the $\mathcal{D}_i$ (for $i = \perp, \parallel, 0+t$) form factors in some more detail with regard to the twist-expansion, the α_s-corrections and the three-particle DA contribution. The parameter that controls in practice the smallness of the $\mathcal{D}_i$ is the heavy quark mass. We therefore investigate the heavy quark scaling by using the standard (heuristic) scaling prescriptions (c.f. [2] for references and details of implementation). At the level of all explicit calculations in the literature it is found that[2] $T_1(0) \sim V(0)|_{\text{twist-2,3}} \sim m_b^{-3/2}$ and $T_1(0) \sim V(0)|_{\text{twist-4}} \sim m_b^{-5/2}$. The derivative form factors follow $\mathcal{D}_1(0)|_{\text{twist-2,3}} \sim m_b^{-5/2}$ [2] which is in agreement with the findings of Charles et al [3]. For this work we have explicitly checked that $\mathcal{D}_1(0)|_{\text{twist-4}} \sim m_b^{-7/2}$ is suppressed and therefore indicates that the twist-expansion of the derivative form factors is well-behaved. The m_b-hierarchy is formally broken by radiative corrections $\mathcal{D}_1(0) \sim O(\alpha_s) m_b^{-3/2}$ which is in accord with the results of Beneke and Feldmann [4]. For LCSR these corrections turn out to be relatively small as can be inferred from the plots. The contribution of the 3-particle DA to the form factor T_1 is about 2% and at the subpercent level for V which means that the contribution to $\mathcal{D}_1$ must be about 2% in order to obey the eom. This is due to the leading twist-3 3-particle DA not contributing to the vector form factors as can be inferred from the formulae given in the appendix in [1]. In particular this means that the closeness of $r_\perp$ to one is accidental as a result of cancellation of the 3-particle DA and the 2-particle DA contributions.

[2] It is well-known that the twist-3 part has the same m_b-scaling, presumably as a result of the Feynman mechanism.

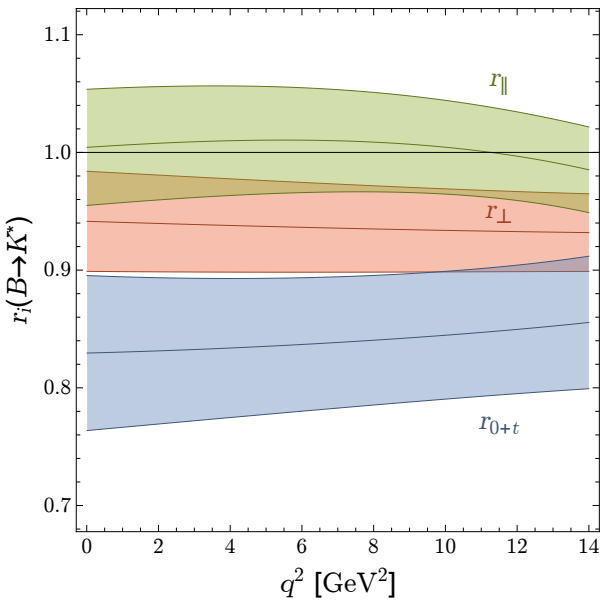

Figure 1: Plots of $r_\perp$, $r_\parallel$ and r_0 eq. (11) (for the $B \to K^*$-transition) as a function of q^2. The deviation from unity is a measure of the relative size of the derivative form factor with respect to the tensor and vector form factors. The mass used in (11) is the pole mass, an issue discussed in appendix A.5. For the explicit m_b mass we use the central value and do not include en error since in the $B \to V\ell\ell$ helicity amplitudes m_b-pole is not present. More precisely an explicit m_b-$\overline{\rm MS}$ is present in front of the tensor form factors. The fact that the quantities tend towards one for very high q^2 is expected from the viewpoint of the Isgur-Wise relations and proves a certain robustness of the LCSR-results for high q^2.

The aspect of the correlation between the continuum thresholds is discussed in some more detail in appendix A.1 (in particular appendix A.5). Here we just summarise the main argument and result. Based on the eom we argue, conservatively, that the continuum thresholds for tensor and vector form factor cannot differ by more than $1\,\text{GeV}^2$ in order for the continuum thresholds of the derivative form factor not to take on absurd low or high values. This argument is less compelling for the $(0+t)$-direction, as can be inferred from the plots, resulting in lower correlation and larger error bands. We stress that if we were to impose standard error bands, say $s_0 = 35(2)\,\text{GeV}^2$ for the sum rule of the $\mathcal{D}_i$ form factors then the error bands for r_i-ratios would shrink to around 1%.

2.3. Discussion of non-resonant background effects

The signal final state in a $B \to \rho(\to \pi\pi)\ell\nu$-type decay, serving as a template decay for any $B \to V\ell_1\ell_2$ decay, is $\pi\pi\ell\nu$. Hence in principle the decay ought to be analysed via a $B \to \pi\pi$ type form factor.[3] The analysis of $B \to \rho\ell\nu$ therefore becomes a matter of how background, finite width and S,P-wave effects are treated or discerned. This question arises in any theoretical computation as well as in any experimental measurement. It is therefore important that both theory and experiment treat these issues in a consistent way.

[3] Within the framework of LCSR this could be done by using the a two-pion DA [16–19]. The technology for pursuing a $B \to \pi\pi$ form factor computation on the lattice has been put forward recently in reference [20].

Let us contrast the ρ final state with the $\pi\pi$-state from a pragmatic viewpoint relevant for this paper. The orbital angular momentum of the $\pi\pi$-state is either $l = 0, 1, ..$ $(S, P, ..$-wave). If the $\pi\pi$-state originates from a ρ-meson then it is necessarily in a P-wave state and shows a distinct angular distribution. Hence this contribution can be separated through an angular analysis from other type of l-waves.[4] We conclude that the S-wave contribution is not to be included in the $B \to \rho$ form factor types and we therefore do not need to attribute any additional uncertainty to it.

We turn to the question of the treatment of the P-wave. From the viewpoint of a ρ-meson there are the issues of the finite width and the non-resonant $\pi\pi$ P-wave background. In an experimental analysis the ρ-meson is though identified with the P-wave $\pi\pi$-signal with invariant two-pion mass $m_{\pi\pi}$ in a certain interval around the ρ-meson peak.[5] Hence in the P-wave itself resonant and non-resonant background are not separated from each other.[6] Our main point of this section is that the very same is the case for the $B \to \rho$ form factors from LCSR and that the treatment is therefore consistent in practice.

Let us argue in some more detail. In current LCSR determinations of the $B \to V$ form factors the V-meson is described by vector meson DAs. The latter are mainly characterised by the longitudinal and transverse decay constants $f_V^{\parallel}$ and $f_V^{\perp}$ respectively and it is therefore important to know how they are obtained. The method of choice for determining $f_V^{\parallel}$ is experiment: $e^+e^- \to V$ (for $V = \rho^0, \phi, \omega$) and $\tau^+ \to V\nu$ (for $V = K^{*,+}, \rho^+$) c.f. appendix of [25] for a discussion. Since the experimental treatment of the ρ-meson versus $\pi\pi$-signal event is the same as for the semileptonic decay $B \to (\rho \to \pi\pi)\ell\nu$ the decay constant effectively includes the non-resonant background. The transverse decay constant $f_V^{\perp}$ is not directly experimentally accessible but is obtained through ratios of $f_V^{\parallel}/f_V^{\perp}$ from lattice QCD and sum rules where one would expect background and finite width effects to cancel to a large extent.

A similar argument can be made from the viewpoint of a computation using a two-pion DAs instead of a ρ DAs. Let us consider for example the contribution of DA that couples to the vector current. The latter is described at lowest order in the conformal spin by the ρ decay constant times the well-known asymptotic DA. From the formulae in [17] it is seen that the analogue of the two-pion DA is given by the pion form factor $f_+^{(\pi)}(q^2)$ times the asymptotic DA. Somewhat symbolically the transitions are then given by

$$\text{vector } \rho\text{−DA}: \qquad f_\rho^{\parallel} \cdot \text{BW}(m_{\pi\pi}^2) \to \frac{f_\rho^{\parallel} m_\rho g_{\rho\pi\pi}}{m_{\pi\pi}^2 - m_\rho^2 - i m_\rho \Gamma_\rho}\,, \tag{12}$$

$$\text{vector } \pi\pi\text{−DA}: \qquad f_+^{(\pi)}(m_{\pi\pi}^2) \qquad \to \frac{f_\rho^{\parallel} m_\rho g_{\rho\pi\pi}}{m_{\pi\pi}^2 - m_\rho^2 - i m_\rho \Gamma_\rho}\,, \tag{13}$$

for $m_{\pi\pi}^2 \simeq m_\rho^2$ where $g_{\rho\pi\pi}$ is the $\rho \to \pi\pi$ decay constant and BW stands for some type of Breit-Wigner ansatz. In both cases there ought to be a local background from non-resonant $\pi\pi$-states. Our argument is that unless one is specifically interested in the local $m_{\pi\pi}^2$-behaviour this contribution can and is effectively absorbed into $f_\rho^{\parallel}$ upon integration over the ρ mass

[4] The importance of separating the S-wave, in the context of $B \to K^*\ell\ell$-type decays, was emphasised not long ago in [21]. Thereafter the S-wave form factors $B \to (K\pi)_{\text{S-wave}}$ were computed in LCSR in the tree level approximation [22].

[5] The choice of the interval is corrected for by the line shape of the ρ-meson.

[6] In the cases where a background has been searched for in $B \to \rho\ell\nu$, it has been found to be consistent with zero [23, 24]. Whether or not future experiments can discern the background is difficult for us to judge but we shall argue that from a pragmatic point of view this might not be necessary.

	$f^{\parallel}$[GeV]	$f^{\perp}$[GeV]	$a_2^{\parallel}$	$a_2^{\perp}$	$a_1^{\parallel}$	$a_1^{\perp}$	$\zeta_3^{\parallel}$ [31]
ρ	0.216(1)(6)	0.160(11)	0.17(7)	0.14(6)	–	–	0.030(10)
ω	0.187(2)(10)	0.139(18)	0.15(12)	0.14(12)	–	–	idem
K^*	0.211(7)	0.163(8)	0.16(9)	0.10(8)	0.06(4)	0.04(3)	0.23(8)
ϕ	0.235(5)	0.191(6)	0.23(8)	0.14(7)	–	–	0.24(8)

Table 1: Scale dependent quantities, e.g. $f^{\perp}$, $a_{1,2}^{\parallel,\perp}$ and $\zeta_3^{\parallel}$, are evaluated at $\mu_F = 1\,\text{GeV}$. In the computation they are scaled by leading log approximation. Input parameters for the light meson DA parameters are the same as in [32] where we have added the three particle DA-parameter $\zeta_3^{\parallel}$. Some more detail on the selection of parameters can be found in that reference. For completeness we have given those for the ω-meson as well. It is noteworthy that the value of $f_{K^*}^{\parallel}$ has changed as compared to previous [25] since the PDG value $\mathcal{B}(\tau \to K^*\nu_\tau) = 1.20(7)\cdot 10^{-2}$ [33] has changed considerably as compared to 2006 $\mathcal{B}(\tau \to K^*\nu_\tau) = 1.29(5)\cdot 10^{-2}$.

window in the experimental analysis. For higher order conformal spin corrections, i.e. higher Gegenbauer moments, and other decay constants the same reasoning applies. This also makes it clear that the non-resonant and resonant background give raise to the same helicity hierarchies for fixed $m_{\pi\pi}$-value. The strong rescattering phases in the $\pi\pi$-channel are universal in each l-wave and do not distort the result.

In summary, in practice the $\rho(\to \pi\pi)$-meson state includes the non-resonant background in the experimental as well as the LCSR prediction. It therefore seems that in practice the uncertainty is a small fraction of the the P-wave background which itself is roughly 5%.[7] In view of all other sizeable uncertainties we refrain from adding any further error due to this effect and reemphasise the importance of comparing our result only with the P-wave contribution of the corresponding $\pi\pi$-pair. Whereas the analysis in this section questions the practical impact of using a two-pion DA around the the ρ-meson mass, it is of course interesting to look at the B_{ℓ_4} decay $B \to \pi\pi\ell\nu$ in other regions of phase space. For recent theoretical developments of B_{ℓ_4} we refer the reader to [28,29] which are though not yet at the level of maturity of K_{ℓ_4} [30].

2.4. Input parameters and uncertainties

The uncertainty of the LCSR results for the form factors is determined from the uncertainties on the input parameters, the factorisation scale μ_F and the Borel parameter M^2 as well as the effective continuum threshold s_0. The values of input parameters used in our calculation, along with the errors assigned can be found in table 1. We draw the reader's attention to the fact that it is the quantity $F(q^2) \cdot f_B$, where F stands for any of the seven form factors, that is determined from the correlation function. Therefore one needs to divide by f_B in order

[7] Despite this aspect it is of interest to estimate the non-resonant background. One can get an idea by analysing the pion form factor $f_+^{(\pi)}(q^2)(p_1 - p_2)_\mu = \langle \pi(p_1)\pi(p_2)|j_\mu^{\text{em}}|0\rangle$. A measure of the non-resonant background around the ρ-meson peak is given by the difference of the model-independent determination of the pion form factor using data on $\pi\pi$-scattering phase shifts and the Omnès-dispersion relation versus a fitted ρ-meson Breit-Wigner ansatz. Around the ρ-meson mass window the difference is found to be 5%. [26]. This is of the same order as the S-wave background found in $B \to \pi\pi\ell\nu$ [27].

to obtain the form factor F. It is well-known and appreciated that the uncertainty in α_s is considerably reduced when sum rule in f_B is taken to same order as for the quantity Ff_B. For example f_B increases by $\sim 9\%$ at $\mathcal{O}(\alpha_s^2\beta_0)$ whereas the combination $(f_+^{B\to\pi} f_B)_{\rm LCSR}/(f_B)_{\rm SR}$ only increases by 2% [34]. Therefore we make use of the QCD sum rules result at $\mathcal{O}(\alpha_s)$ [35,36] for f_B.

The two sum rule specific parameters are the Borel parameter M^2 and the effective continuum threshold s_0. For reasons of consistency the Borel parameter is to be chosen at an extremum (c.f. appendix A.6) which serves as a quality control parameter. The continuum threshold is more problematic and the final result does depend on the choice. Hence our recipe for the error analysis is to assume a sizeable uncertainty for the continuum threshold. The new ingredient of our analysis is that we have argued that the eom results in correlations between the continuum thresholds; (c.f. appendix A.2 for an elaborate discussion). The correlations used are summarised in and in between eqs. (A.8) and (A.9). More precisely the correlation of the continuum thresholds is such that their relative uncertainty is $1\,\text{GeV}^2$ which has to be compared to their individual uncertainty of $2\,\text{GeV}^2$ or the uncertainty of their sum which is close to $4\,\text{GeV}^2$. The influence of the Borel parameter on the light-cone sum rule is negligible as compared to the continuum threshold of the light-cone sum rule and we therefore do not vary them separately for each form factor. The Borel parameter dependence of the f_B-sum rule is sizeable and is taken into account and contributes to the uncertainty of the normalisation of the form factors. The intermediate states in the light-cone and the f_B sum rule are the same since they couple to the same interpolating current J_B. It would therefore seem absurd, or contradictive to the method, if the corresponding continuum thresholds were far apart. We implement this reasoning by correlating $s_0^{f_B}$ and $s_0^{\rm LC}$ at the 50%-level which implies that the uncertainty on the difference is $2\,\text{GeV}^2$; a factor of $\sqrt{2}$ lower than without correlation.

We turn to the choice of the actual central values of the continuum threshold and the Borel parameter. It is useful to recall that if the sum rules were perfect then the LCSR form factor would be independent of the Borel parameter. In reality a small Borel parameter is desirable from the viewpoint of suppressing any higher states in the spectrum whereas a large Borel parameter improves the convergence of the light-cone operator product expansion (LC-OPE). In practice one therefore chooses a compromise value which is usually found as an extremum. The flatness of the form factor around this extremum as a function of the Borel parameter is a measure of the quality of the sum rule. In appendix A.6 it is shown that extremizing in the Borel parameter is formally equivalent to imposing a daughter sum rule for m_B^2. From the viewpoint of the physics, the effective continuum threshold is expected to lie somewhere between $(m_B + 2m_\pi) \simeq 30.9\,\text{GeV}^2$ and $(m_B + m_\rho)^2 = 36.6\,\text{GeV}^2$ with the true value being closer to the latter since the production of a ρ-meson is much more likely than the production of two non-resonant pions. Furthermore we verify that the contribution of the highest twist term does not exceed 10%. The latter assures convergence of the light-cone or twist-expansion respectively. More precisely we compare the twist-4 tree level contribution to the remaining tree level contribution. In order to limit contamination due to higher states we verify that the continuum contribution does not exceed 30%. If one assumes that semi-global quark hadron-duality itself works at the 30%-level the additional suppression reduces this error to just below the 10%-level. The sum rule parameters, with some more details in the caption, are given in the table 2.

B_q	$M^2_{f_{Bq}}$	$s_0^{f_{Bq}}$	$M^2_{\rm LC}$	$s_0^{\rm LC}$
B_d	4.1(1)	34.2(2)	$c_c/\langle u\rangle_{q^2} M^2_{f_{B_d}}$	35(2)
B_s	4.4(1)	35.4(2)	$c_c/\langle u\rangle_{q^2} M^2_{f_{B_s}}$	36(2)

Table 2: Sum rule parameters for B_d and B_s sum rules. All numbers are in units of GeV^2, $M^2_{f_B(\text{LC})}$ and $s_0^{f_B(\text{LC})}$ denote the Borel parameter and continuum threshold of the f_B sum rule and the LCSR of $f_B F(q^2)$ (where F stands for a form factor) respectively. The difference between the B_d and B_s continuum thresholds follows $(m_{B_d}+\Delta)^2 = s_0|_{B_d}$ and $(m_{B_s}+\Delta)^2 = s_0|_{B_s}$. The average momentum fraction of the transition quark $\langle u\rangle_{q^2}$ (c.f. [37] for the definition) varies smoothly from 0.86 at $q^2 = 0\,\text{GeV}^2$ to 0.77 at $q^2 = 14\,\text{GeV}^2$. Dividing the sum rule parameter by this quantity serves to take into account q^2-dependence the Borel parameter under the extremisation procedure. The value $c_c = 2.2$ is determined through the mentioned procedure of extremisation. The criteria in the text imply that the Borel parameter of the LCSR is considerably higher than that from the f_B-sum rule [37].

F_i	J^P	$m_{R,i}^{b\to d}/\,\text{GeV}$	$m_{R,i}^{b\to s}/\,\text{GeV}$
A_0	0^-	5.279	5.366
T_1, V	1^-	5.325	5.415
$T_{2,23}, A_{1,12}$	1^+	5.724	5.829

Table 3: Masses of resonances of quantum numbers J^P as indicated necessary for the parameterisation of form factor F_i for $b\to d$ and $b\to s$ transitions.

2.5. Series expansion fits to LCSR form factors

As mentioned in the introduction, for phenomenological analyses of rare decays, it is crucial to take into account the theoretical uncertainties of the $B\to V$ form factors and the correlations among them. In order to facilitate the use of the LCSR results, we perform fits of the full analytical result to a simplified series expansion (SSE), which is based on a rapidly converging series in the parameter

$$z(t) = \frac{\sqrt{t_+ - t} - \sqrt{t_+ - t_0}}{\sqrt{t_+ - t} + \sqrt{t_+ - t_0}} \tag{14}$$

where $t_\pm = (m_B \pm m_V)^2$ and $t_0 = t_+(1-\sqrt{1-t_-/t_+})$. We write the form factors as

$$F_i(q^2) = P_i(q^2) \sum_k \alpha_k^i \left[z(q^2) - z(0)\right]^k , \tag{15}$$

where $P_i(q^2) = (1-q^2/m^2_{R,i})^{-1}$ is a simple pole corresponding to the first resonance in the spectrum. The appropriate resonance masses are given in table 3. We consider fits that are truncated after the quadratic term in z, i.e. we will have three fit parameters $\alpha_{0,1,2}$ for each of the seven form factors. We will see in sec. 2.6 that a three-parameter fit is sufficient for a combined fit to lattice and LCSR results in the entire kinematic range relevant for $B\to V\ell^+\ell^-$ decays.

	$B \to K^*$	$B \to \rho$	$B \to \omega$	$B_s \to \phi$	$B_s \to K^*$
$A_0(0)$	0.391 ± 0.035	0.369 ± 0.034	0.311 ± 0.040	0.433 ± 0.035	0.336 ± 0.032
$A_1(0)$	0.289 ± 0.027	0.267 ± 0.025	0.237 ± 0.031	0.315 ± 0.027	0.246 ± 0.023
$A_{12}(0)$	0.281 ± 0.025	0.307 ± 0.028	0.257 ± 0.033	0.274 ± 0.022	0.246 ± 0.023
$V(0)$	0.366 ± 0.035	0.333 ± 0.032	0.296 ± 0.039	0.407 ± 0.033	0.311 ± 0.030
$T_1(0)$	0.308 ± 0.031	0.281 ± 0.026	0.250 ± 0.035	0.331 ± 0.030	0.254 ± 0.027
$T_2(0)$	0.308 ± 0.031	0.281 ± 0.026	0.250 ± 0.035	0.331 ± 0.030	0.254 ± 0.027
$T_{23}(0)$	0.793 ± 0.064	0.807 ± 0.080	0.696 ± 0.081	0.763 ± 0.061	0.643 ± 0.058

Table 4: Values of the form factors at $q^2 = 0$ and their uncertainties.

Note that the parameterisation (15) as used in ref. [38] differs from that used in [39]. It has the advantage that the value of the form factor at $q^2 = 0$ is among the fit parameters, $F_i(0) = \alpha_0^i$. We prefer this parameterisation as it allows to impose the exact kinematical relations $A_0(0) = (8 m_B m_V)/(m_B^2 - m_V^2)\, A_{12}(0)$ and $T_1(0) = T_2(0)$ at the level of the SSE coefficients as

$$\alpha_0^{A_0} = \frac{8 m_B m_V}{m_B^2 - m_V^2}\, \alpha_0^{A_{12}}\,, \qquad\qquad \alpha_0^{T_1} = \alpha_0^{T_2}\,. \tag{16}$$

The results for the form factors at $q^2 = 0$ are provided in table 4. To determine the fit coefficients α_i, their uncertainties, and the correlations between them, we first generate an ensemble of N input parameter sets where the values of the input parameters are randomly distributed according to a multivariate normal distribution with the location given by the central values and the covariance given by the uncertainties and correlations of the input parameters discussed above. We then compute all form factors at different steps of q^2 between 0 and 10 GeV^2. Finally, we fit the z expansion to all seven form factors for the N ensembles of form factor values and extract the mean, variance, and correlation of the z expansion coefficients $\alpha_{0,1,2}$.

The resulting mean and variance are shown in table 11. We do not reproduce the full 21×21 correlation matrices in the paper but rather provide them as ancillary files downloadable available from the arXiv preprint page (see appendix D for details). Here we merely note that these correlations are sizeable and it is crucial to include them when using the form factors in phenomenological analyses.

With these results at hand, the uncertainty of an observable Ψ (e.g. angular observable) can be computed via

$$\sigma^2(\Psi) = \sum_{k,l,i,j} \frac{\partial \Psi(F_i)}{\partial \alpha_k^i}\, \mathrm{cov}(\alpha_k^i, \alpha_l^j)\, \frac{\partial \Psi(F_i)}{\partial \alpha_l^j}\,. \tag{17}$$

where $i, j = 1 \ldots 7$ denotes the form factor index and $k, l = 0 \ldots 2$ parameterises the expansion coefficients of the z-series. The covariance matrix is defined as

$$\mathrm{cov}(\alpha_k^i, \alpha_l^j) = \mathrm{corr}(\alpha_k^i, \alpha_l^j)\, \sigma(\alpha_k^i)\, \sigma(\alpha_l^j) \qquad \text{(no sums)} \tag{18}$$

in terms of the correlation matrix and the variances.

2.6. Interpolating between lattice and LCSR form factors

The LCSR and lattice form factor calculations are complementary since the former is valid at low q^2 and the latter at high q^2. Performing a combined fit of the SSE parameterisation to both lattice and LCSR results is useful for two reasons. First, whether a good fit to two completely independent methods in two different kinematical regions is possible at all is a powerful consistency check of those methods. Second, in phenomenological analyses constraining physics beyond the SM combining both observables at low and at high q^2, one needs a consistent set of form factors for the full q^2 range.

To obtain this combined fit, we first generate pseudo-data points with correlated theoretical uncertainties at three q^2 values both at low and at high q^2. For LCSR at low q^2, we proceed as in the previous subsection. For the lattice form factors at high q^2, we make use of the parameterisation of lattice form factors provided in [39]. We generate an ensemble of series expansion coefficient sets randomly distributed according to a multivariate normal distribution, using the fitted central values and covariance given in [39]. For each of the sets, we then evaluate the form factors at the three q^2 values and extract the uncertainties and correlation of these pseudo-data points.

We then construct a χ^2 function

$$\begin{aligned}\chi^2(\alpha_0^1,\ldots,\alpha_2^7) = &\\ &+\sum_{ijkl}\left[F^i_{\rm LCSR}(q_k^2)-F^i_{\rm fit}(q_k^2;\alpha_m^i)\right](C^{ijkl}_{\rm LCSR})^{-1}\left[F^j_{\rm LCSR}(q_l^2)-F^j_{\rm fit}(q_l^2;\alpha_n^j)\right]\\ &+\sum_{ijkl}\left[F^i_{\rm latt}(q_k^2)-F^i_{\rm fit}(q_k^2;\alpha_m^i)\right](C^{ijkl}_{\rm latt})^{-1}\left[F^j_{\rm latt}(q_l^2)-F^j_{\rm fit}(q_l^2;\alpha_n^j)\right] \quad (19)\end{aligned}$$

where F^i_X are the central values of the pseudo data points of form factor i and C^{ijkl}_X the corresponding covariance matrices (taking into account both the correlation between different form factors and different q^2 values). We then sample a likelihood $L = e^{-\chi^2/2}$ using a Markov Chain Monte Carlo (MCMC) approach with flat priors for the series expansion coefficients. From the stationary distribution of the MCMC, we extract the central values and covariance of the coefficients.

Fig. 2 shows the fit result for the $B \to K^*$ form factors in the variable q^2. The form factor plots, in the $z(q^2)$-variable, for the modes $B \to K^*$, $B_s \to \phi$ and $B_s \to \bar{K}^*$ are shown in figs. 5,6,7 of appendix C. The LCSR and lattice pseudo-data points are shown in blue and red. The light red dashed band shows the 2-parameter fit from [39]. The solid gray band is our combined 3-parameter fit result. The numerical fit coefficients, of both fits, are reproduced in table 12 in appendix D. As for the pure LCSR fit, the central values, the uncertainties and all correlations are provided as ancillary files on the arXiv preprint page (see appendix D).

We would like to add that the fits are valid under the premise that the LCSR and lattice QCD data points and their uncertainties, including correlations, are valid as well as the z-expansion being a reasonable model function. There is no evidence against the latter, as we have found that adding higher orders in the z expansion and using different parameterisations does not change matters. This is an aspect that could change in the future with more precise form factor determination from LCSR and or lattice QCD. Overall the agreement is good, at the exception of T_{23}. This was already noted in [39] where the LCSR were compared to an extrapolation of the lattice predictions to low q^2. The fits in the $z(q^2)$-variable, shown in figs. 5,6,7, are particularly useful in judging the quality of the fits. In these figures the form

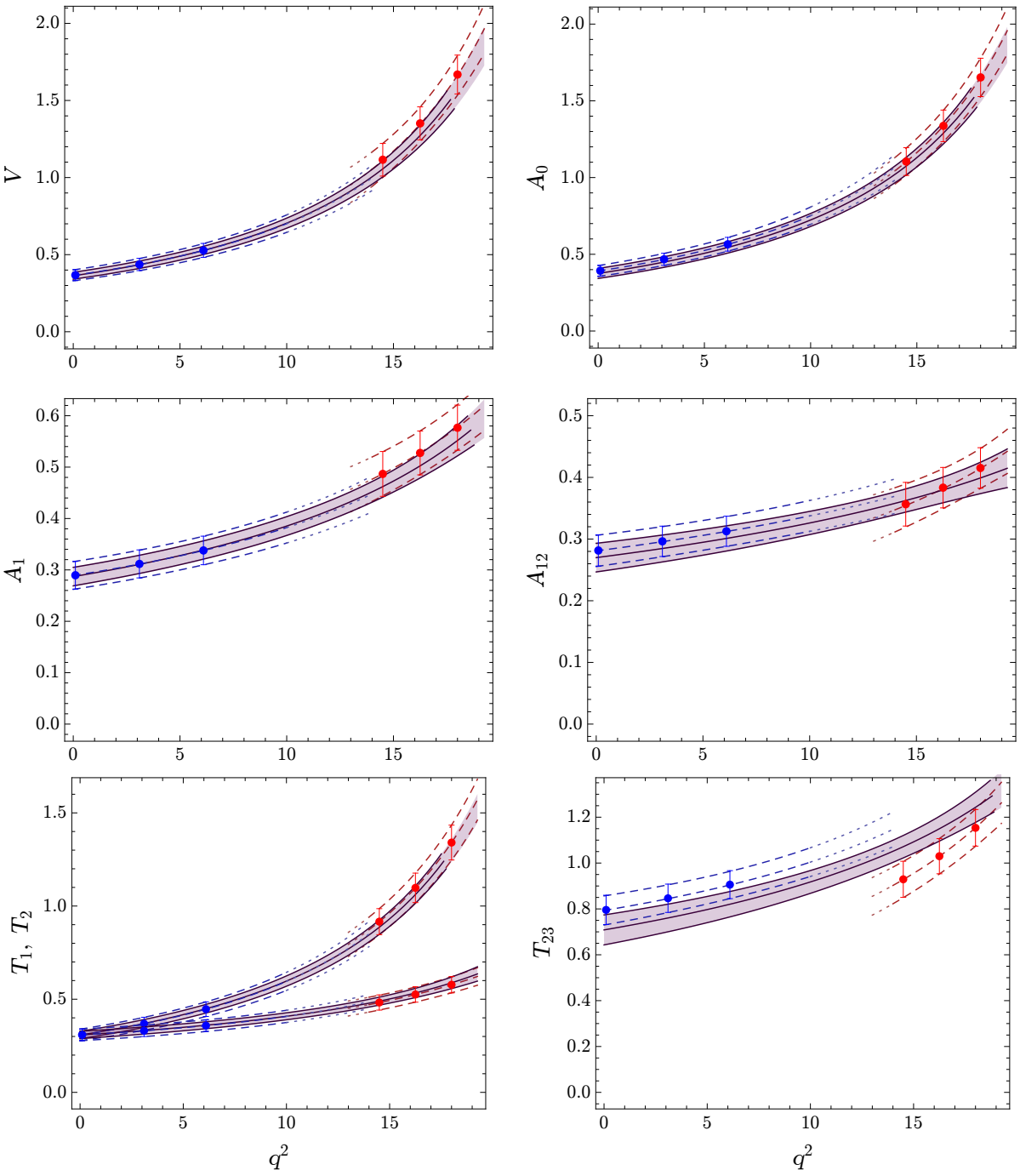

Figure 2: Combined LCSR and lattice fit to $B \to K^*$ form factors, where lattice data points are indicated in red, LCSR points in blue, the gray solid band shows the combined 3-parameter fit and the red dashed band the 2-parameter lattice fit from ref. [39].

factors times $P = (q^2 - m_R^2)$ is plotted. The latter serves to cancel the first physical pole, at the resonance R, in the q^2-spectrum. The remaining slope therefore is a measure of the behaviour of the higher poles or cuts in the q^2-spectrum.

An interesting qualitative feature is the behaviour of the $B \to K^*$ versus $B_s \to \phi$ lattice form factors $P \cdot T_{23}(q^2)$ (and to some extent also $P \cdot A_{12}$). From figs. 5,6 is seen that the slopes are opposite in direction for the two cases. In a LCSR computation, valid at low q^2, such a qualitative difference cannot arise since the main difference between $B \to K^*$ versus $B_s \to \phi$ form factor is due to hadronic input data (which is numerically similar). It is possible that by going closer to the hadronic spectrum, at high q^2, a more distinct pattern arises in accordance with the lattice QCD computation. It will be interesting to see whether this qualitative feature which is not yet statistically significant is confirmed in future lattice predictions with higher statistics and a more complete treatment of the vector mesons (e.g. physical quark masses).

To this end we would like to add that differences in normalisation of $\parallel, \perp$ (V, A_1 and $T_{1,2}$) versus 0-helicity (A_0 A_{12} and T_{23}) in the LCSR computation are highly sensitive to f_V and f_V^T decay constants. For instance the 0-helicity form factors depend to $\sim 75\%$ on the normalisation of f_V with the situation being just the opposite for the $\parallel, \perp$-helicity form factors.

3. Phenomenological applications

We make use of the updated form factors and their error correlations in predicting experimentally accessible observables. More specifically we consider the flavour changing neutral current transitions (FCNC) $b \to s$ $B \to K^* \mu^+ \mu^-$, $B \to K^* \gamma$, $B_s \to \phi \mu^+ \mu^-$ sensitive to physics beyond the SM and the branching fractions of the tree-level decays $B \to (\rho, \omega) \ell \nu$. The latter are of interest to extract the CKM matrix element $|V_{\rm ub}|$ and conversely serve as a test of the form factor normalisation (and shape) when $|V_{\rm ub}|$ is taken as an input from other channels and global fits.

3.1. $B \to K^* \mu^+ \mu^-$ at low q^2

The decay $B \to K^* \mu^+ \mu^-$, being one of the golden channels of LHCb, requires no introduction. It has received a great deal of attention, particularly in the last decade. By making use of the large energy relation [3], observables have been identified which have reduced uncertainties with respect to to form factors (e.g [6]). Recent measurements of several of these observables by LHCb [40–42], CMS [43], and ATLAS [44] have revealed a number of potential tensions with the SM predictions. Whether or not this is due to new physics or hadronic effects is a subject of vital debate [5, 45–50]. This motivates reinvestigation into predictions of hadronic quantities such as the form factors undertaken in this work.

In the SM, neglecting the muon mass, the differential decay distribution of $B \to K^* \mu^+ \mu^-$ can be written in terms of of six helicity amplitudes

$$H_\iota^V = N \sqrt{q^2} \left(C_9^{\rm eff}(q^2)\, \mathcal{V}^{(\iota)}(q^2) + \frac{2 m_b}{q^2}\, C_7^{\rm eff}(q^2)\, T^{(\iota)}(q^2) + i \sqrt{\lambda}\, \frac{2 m_b}{q^2}\, \Delta_\iota(q^2) \right), \tag{20}$$

$$H_\iota^A = N \sqrt{q^2}\, C_{10}\, \mathcal{V}^{(\iota)}(q^2), \tag{21}$$

where $\iota = +, -, 0$ denotes the polarisation of the K^*-meson. The helicity form factors $T^{(\iota)}, \mathcal{V}^{(\iota)}$ are defined as in appendix B and Δ_ι stands for various corrections to be discussed further below.

The quantity

$$N \equiv V_{tb}V_{ts}^* \left[\frac{G_F^2\alpha^2}{3\cdot 2^{10}\pi^5 m_B^3}\lambda^{1/2}\right]^{1/2}, \tag{22}$$

is a normalisation factor where G_F stand for Fermi's constant, e for the electric charge and $V_{\mathrm{tb(s)}}$ are CKM matrix elements. The differential branching ratio is then given by

$$\frac{d\mathrm{BR}(B_q \to K^*\mu^+\mu^-)}{dq^2} = \tau_{B_q}\frac{1}{2}\sum_{\iota=\pm,0}\sum_{X=V,A}|H_\iota^X|^2\,. \tag{23}$$

Factorisable quark loop contributions are absorbed into Wilson coefficients C_7^{eff} and C_9^{eff} which therefore become q^2-dependent (e.g. [51] for the definition). The quantities Δ_ι contain the NNLL corrections to the matrix elements of the current-current operators [52] as well as various "non-factorisable" contributions. The latter entail the effect of weak annihilation, the chromomagnetic operator contribution both computed in LCSR [7,53] as well as hard spectator scattering taken from QCD factorisation [54, 55].

An important contribution arises due to the final state leptons emerging from charm quarks; so called charm loops. At high q^2 the effect of the broad charmonium resonances measured by the LHCb-collaboration [56] has turned out to be substantially more sizeable than anticipated [48]. It therefore seems well-motivated to discuss the various contributions in some detail. At low $q^2 < 6\,\mathrm{GeV}^2$ such effects are thought to be captured in the partonic language of charm quarks and gluons. The $O(\alpha_s)$ hard vertex corrections [52] factorise in the heavy quark limit into a q^2-dependent function times the form factor. The part which does not contain gluon exchanges between the hadron transition and the charm loop factorises non-perturbatively by definition and the q^2-dependent function is given by the vacuum polarisation. The latter can be extracted in a model-independent way from $e^+e^- \to$ hadrons-data.[8] These contributions, as mentioned above, are included in the central values of the predictions of our work. In addition there is soft gluon emission from the charm loop into the B-meson as well as the K^*-meson. Both effects have been assessed in LCSR, the former with a B-meson DA [57] and the latter with K^*-meson DA (for $B \to K^*\gamma$ only) [25, 58]. The combination of the two results is not completely free from model-dependence.[9] At q^2 approaching the charmonium resonance region, the contribution is predicted to be significantly enhanced, rendering the partonic theory prediction unreliable above about 6 GeV^2. These two effects, the soft gluon emission and the charmonium effect, can be captured in the region $q^2 \in [0, 6\,\mathrm{GeV}^2]$ by a linear parameterisation

$$\Delta_\iota^{c\bar{c}}(q^2) = \frac{i}{\sqrt{\lambda}}C_7^{\mathrm{eff}}T^{(\iota)}\left[a_\iota e^{i\phi_{a_\iota}} + b_\iota e^{i\phi_{b_\iota}}\left(\frac{q^2}{6\,\mathrm{GeV}^2}\right)\right], \tag{24}$$

where a, b are positive numbers and $\phi_{a,b}$ are strong phases whose parameter ranges we discuss further below. Note that (24) and the replacement of

$$C_7^{\mathrm{eff}} \to C_7^{\mathrm{eff}}\left[1 + a_\iota e^{i\phi_{a_\iota}} + b_\iota e^{i\phi_{b_\iota}}\left(\frac{q^2}{6\,\mathrm{GeV}^2}\right)\right] \tag{25}$$

[8] C.f. [48] for a recent determination.

[9] The problem is that the two effects are computed in two, slightly, different frameworks. It would be best two compute, in either of the two frameworks, the radiative corrections which would then include both effects as well as the $O(\alpha_s)$ vertex corrections. This is though a rather challenging.

in (20) are equivalent to each other. The parameterisation (24) is convenient for low q^2 since it incorporates the helicity hierarchy $\Delta_+ \ll \Delta_-$[10] through the form factor parameterisation. This results in $a_+ \simeq a_-$ and $b_+ \simeq b_-$. We find[11]

$$\begin{aligned} a_\pm &\in [0, 0.05] \,, \quad b_\pm \in [0, 0.2] \,, \\ a_0 &\in [0, 0.2] \,, \quad\quad b_0 \in [0, 0.05] \,. \end{aligned} \tag{26}$$

where a_ι is mainly fixed at low q^2 by the soft gluon emission [25,57,58] and b_ι is then determined to cover the J/Ψ uncertainty. More precisely we vary the phase of the J/Ψ-residue in the dispersion representation in the full range motivated by the findings in [48]. Note the absolute value of the residues are known from the polarisation specific branching fractions $B \to J/\Psi K^*$. The asymmetry between the parameter values of a_0, b_0 and $a_\pm, b_\pm$ originates from the fact that $\pm$ directions, contrary to the 0-helicity direction, are sensitive to the photon pole $1/q^2$. At intermediate q^2 this hierarchy disappears which can for example be seen from the polarisation fractions of the $B \to J/\Psi K^*$ amplitudes and or the general result that the helicity amplitudes are degenerate at the kinematic endpoint [60]. In summary the uncertainty to soft gluon emission and nearby resonances is covered by the parameterisation (25) with parameter ranges as given in (26) and varying the phases $\phi_{a,b}$ in the full range.

Numerical predictions in different q^2 bins for $B^0 \to K^{*0}\mu^+\mu^-$ observables (see e.g. refs. [6,51] for definitions of the angular observables) and the $B^+ \to K^{*+}\mu^+\mu^-$ branching ratio are given in tables 5, 6 and 7 respectively. Crucially uncertainties are split into parametric[12], form factor and non-factorisable charm uncertainties as parameterised in eq. (24). It is observed that the dominant uncertainty of the branching fraction is due to form factors and amounts to about 12% relative to the central value. In the case of the angular observables the error is considerably reduced by the inclusion of the correlations. Comparing the angular observables $S_{4,5}$ with the related observables $P_{4',5'}$ it is noted that the form factor uncertainties are comparable. This improvement for $S_{4,5}$ observables is due to the inclusion of correlated uncertainties. The error due to the Δ-corrections results in comparable uncertainties in both bases.

For comparison of the $B \to K^*\mu^+\mu^-$ observables to existing experimental measurements of 1fb^{-1}LHCb-data and the implications for new physics, we refer the reader to [49], where the form factor results of this work were used for a global analysis of $b \to s$ transitions.

3.2. $B \to K^*\gamma$

The precise experimental determination of the branching ratio for $B \to K^*\gamma$ provides a good opportunity to compare our results for the form factors to experiment. The branching ratio of $B \to K^*\gamma$ is given by

$$\text{BR}(B_q \to K^*\gamma) = \tau_{B_q} 48\pi^2 \left(|H_+^q|^2 + |H_-^q|^2\right) \,, \tag{27}$$

where $q = u, d$. We have introduced the superscript q in addition to the previous section because we give separate predictions for charged and neutral modes. The amplitudes are

[10] We refer the reader to the appendix of [53] and [59] for recent theoretical discussions of this topic.

[11] Compared to the parameterisation used in [49] the value of b_0 is considerably reduced. For the observables presented in this paper this effect has a negligible influence on the values of the uncertainty.

[12] The parametric uncertainties, with values adopted from the PDG [33], include $|V_{\text{tb}}V_{\text{ts}}^*| = (4.01 \pm 0.10) \cdot 10^{-2}$, the scale variation $\mu = 4.8 \pm 0.8\,\text{GeV}$, the b-quark $\overline{\text{MS}}$ mass $m_b(m_b) = 4.18 \pm 0.03\,\text{GeV}$ and the pole mass of the charm quark $m_c(m_c) = 1.4 \pm 0.2\,\text{GeV}$.

$B^0 \to K^{*0}\mu^+\mu^-$		
Observable	q^2 bin	SM prediction
$10^7 \, \frac{d\mathrm{BR}}{dq^2}$	$[0.1, 1]$	$1.083 \pm 0.074 \pm 0.151 \pm 0.057$
	$[1, 2]$	$0.511 \pm 0.030 \pm 0.069 \pm 0.017$
	$[2, 3]$	$0.459 \pm 0.027 \pm 0.064 \pm 0.015$
	$[3, 4]$	$0.467 \pm 0.028 \pm 0.062 \pm 0.018$
	$[4, 5]$	$0.494 \pm 0.031 \pm 0.062 \pm 0.023$
	$[5, 6]$	$0.530 \pm 0.036 \pm 0.063 \pm 0.029$
	$[1.1, 2.5]$	$0.488 \pm 0.067 \pm 0.067 \pm 0.015$
	$[2.5, 4]$	$0.464 \pm 0.062 \pm 0.062 \pm 0.017$
	$[4, 6]$	$0.512 \pm 0.063 \pm 0.063 \pm 0.026$
A_{FB}	$[0.1, 1]$	$-0.088 \pm 0.001 \pm 0.009 \pm 0.001$
	$[1, 2]$	$-0.140 \pm 0.003 \pm 0.029 \pm 0.010$
	$[2, 3]$	$-0.078 \pm 0.003 \pm 0.018 \pm 0.019$
	$[3, 4]$	$0.002 \pm 0.003 \pm 0.009 \pm 0.025$
	$[4, 5]$	$0.077 \pm 0.004 \pm 0.018 \pm 0.028$
	$[5, 6]$	$0.144 \pm 0.006 \pm 0.026 \pm 0.030$
	$[1.1, 2.5]$	$-0.124 \pm 0.027 \pm 0.027 \pm 0.013$
	$[2.5, 4]$	$-0.018 \pm 0.009 \pm 0.009 \pm 0.023$
	$[4, 6]$	$0.112 \pm 0.022 \pm 0.022 \pm 0.029$
F_L	$[0.1, 1]$	$0.308 \pm 0.009 \pm 0.053 \pm 0.018$
	$[1, 2]$	$0.738 \pm 0.008 \pm 0.045 \pm 0.021$
	$[2, 3]$	$0.831 \pm 0.002 \pm 0.031 \pm 0.012$
	$[3, 4]$	$0.820 \pm 0.002 \pm 0.034 \pm 0.007$
	$[4, 5]$	$0.776 \pm 0.003 \pm 0.040 \pm 0.012$
	$[5, 6]$	$0.723 \pm 0.004 \pm 0.045 \pm 0.019$
	$[1.1, 2.5]$	$0.776 \pm 0.040 \pm 0.040 \pm 0.018$
	$[2.5, 4]$	$0.825 \pm 0.033 \pm 0.033 \pm 0.007$
	$[4, 6]$	$0.749 \pm 0.043 \pm 0.043 \pm 0.016$

Table 5: Standard model predictions for binned $B^0 \to K^{*0}\mu^+\mu^-$ observables, where the uncertainties are split into parametric uncertainties, form factor uncertainties, and our estimate of the uncertainties due to missing hadronic effects.

$B^0 \to K^{*0}\mu^+\mu^-$		
Observable	q^2 bin	SM prediction
S_4	$[0.1, 1]$	$0.097 \pm 0.000 \pm 0.004 \pm 0.002$
	$[1, 2]$	$0.023 \pm 0.004 \pm 0.008 \pm 0.009$
	$[2, 3]$	$-0.081 \pm 0.004 \pm 0.013 \pm 0.013$
	$[3, 4]$	$-0.151 \pm 0.003 \pm 0.016 \pm 0.013$
	$[4, 5]$	$-0.198 \pm 0.002 \pm 0.016 \pm 0.013$
	$[5, 6]$	$-0.228 \pm 0.001 \pm 0.015 \pm 0.011$
	$[1.1, 2.5]$	$-0.009 \pm 0.009 \pm 0.009 \pm 0.011$
	$[2.5, 4]$	$-0.135 \pm 0.016 \pm 0.016 \pm 0.013$
	$[4, 6]$	$-0.213 \pm 0.016 \pm 0.016 \pm 0.012$
S_5	$[0.1, 1]$	$0.247 \pm 0.002 \pm 0.009 \pm 0.004$
	$[1, 2]$	$0.119 \pm 0.005 \pm 0.015 \pm 0.020$
	$[2, 3]$	$-0.077 \pm 0.005 \pm 0.015 \pm 0.027$
	$[3, 4]$	$-0.212 \pm 0.003 \pm 0.021 \pm 0.028$
	$[4, 5]$	$-0.300 \pm 0.005 \pm 0.023 \pm 0.025$
	$[5, 6]$	$-0.356 \pm 0.006 \pm 0.021 \pm 0.022$
	$[1.1, 2.5]$	$0.059 \pm 0.014 \pm 0.014 \pm 0.023$
	$[2.5, 4]$	$-0.182 \pm 0.020 \pm 0.020 \pm 0.028$
	$[4, 6]$	$-0.329 \pm 0.022 \pm 0.022 \pm 0.024$
P_4'	$[0.1, 1]$	$0.252 \pm 0.003 \pm 0.006 \pm 0.006$
	$[1, 2]$	$0.058 \pm 0.010 \pm 0.019 \pm 0.022$
	$[2, 3]$	$-0.232 \pm 0.012 \pm 0.028 \pm 0.042$
	$[3, 4]$	$-0.413 \pm 0.006 \pm 0.022 \pm 0.035$
	$[4, 5]$	$-0.487 \pm 0.003 \pm 0.017 \pm 0.023$
	$[5, 6]$	$-0.518 \pm 0.002 \pm 0.015 \pm 0.016$
	$[1.1, 2.5]$	$-0.023 \pm 0.023 \pm 0.023 \pm 0.029$
	$[2.5, 4]$	$-0.375 \pm 0.024 \pm 0.024 \pm 0.038$
	$[4, 6]$	$-0.502 \pm 0.016 \pm 0.016 \pm 0.019$
P_5'	$[0.1, 1]$	$0.643 \pm 0.001 \pm 0.009 \pm 0.014$
	$[1, 2]$	$0.297 \pm 0.010 \pm 0.026 \pm 0.041$
	$[2, 3]$	$-0.223 \pm 0.015 \pm 0.041 \pm 0.084$
	$[3, 4]$	$-0.579 \pm 0.011 \pm 0.037 \pm 0.077$
	$[4, 5]$	$-0.738 \pm 0.014 \pm 0.033 \pm 0.057$
	$[5, 6]$	$-0.809 \pm 0.016 \pm 0.031 \pm 0.042$
	$[1.1, 2.5]$	$0.154 \pm 0.032 \pm 0.032 \pm 0.055$
	$[2.5, 4]$	$-0.504 \pm 0.038 \pm 0.038 \pm 0.081$
	$[4, 6]$	$-0.774 \pm 0.032 \pm 0.032 \pm 0.049$

Table 6: Standard model predictions for binned angular $B^0 \to K^{*0}\mu^+\mu^-$ observables, where the uncertainties are split into parametric uncertainties, form factor uncertainties, and our estimate of the uncertainties due to missing hadronic effects.

$B^+ \to K^{*+}\mu^+\mu^-$		
Observable	q^2 bin	SM prediction
$10^7 \ \frac{d\text{BR}}{dq^2}$	$[0.1, 1]$	$1.155 \pm 0.079 \pm 0.161 \pm 0.060$
	$[1, 2]$	$0.555 \pm 0.033 \pm 0.075 \pm 0.018$
	$[2, 3]$	$0.506 \pm 0.029 \pm 0.070 \pm 0.016$
	$[3, 4]$	$0.515 \pm 0.030 \pm 0.068 \pm 0.020$
	$[4, 5]$	$0.544 \pm 0.034 \pm 0.068 \pm 0.026$
	$[5, 6]$	$0.582 \pm 0.040 \pm 0.069 \pm 0.032$
	$[1.1, 2.5]$	$0.533 \pm 0.073 \pm 0.073 \pm 0.016$
	$[2.5, 4]$	$0.511 \pm 0.068 \pm 0.068 \pm 0.019$
	$[4, 6]$	$0.563 \pm 0.068 \pm 0.068 \pm 0.029$

Table 7: Standard model predictions for the differential branching ratio of $B^+ \to K^{*+}\mu^+\mu^-$, where the uncertainties are split into parametric uncertainties, form factor uncertainties, and our estimate of the uncertainties due to missing hadronic effects.

related to the limit of the vector helicity amplitudes of $B \to K^*\ell^+\ell^-$ at vanishing dilepton invariant mass,

$$H_\pm^q(B \to K^*\gamma) = \lim_{q^2\to 0} \frac{q^2}{e} H_\pm^{V,q}(B \to K^*\ell^+\ell^-) \,. \tag{28}$$

They can be written as

$$H_\pm^q = \frac{N}{e}\sqrt{\lambda_0}\left(2m_b\, C_7^{\text{eff}}\,(T_\pm(0) + i\,2\,m_b\,\Delta_\pm^q(0)\right) \,, \tag{29}$$

where and $\lambda_0 = \lambda|_{q2=0} = (m_B^2 - m_{K^*}^2)^2$ is the Källén-function for the photon final state and $T_\pm(0) = T^{(\pm)}(q^2)/\sqrt{\lambda(q^2)}|_{q^2=0}$ which results in $T_+(0) = 2T_1(0)$ and $T_-(0) = 0$. The quantity $T^{(\pm)}$ is defined in appendix B. For $\Delta_\pm(0)$, the following contributions are included,

- Corrections to the matrix elements of current-current operators [52];
- Hard scattering contributions computed in QCD factorisation [54, 55];
- Non-factorisable contributions of the chromomagnetic penguin operator O_8 computed in LCSR [53];
- Weak annihilation computed in LCSR [7].

The first of these corrections is by far the dominant one, leading to a +60% shift in the branching ratios. The three remaining ones contribute to the isospin asymmetry (e.g. [7]) of which WA is the one which is most sizeable.

Our predictions for the branching ratios are listed in table 8 along with the experimental world averages and are consistent with the experimental results. We would like to emphasise that the $B \to K^*\gamma$ is a FCNC and that the consistency cannot be taken to be one to one

	Theory	Experiment
$10^4 \times \mathrm{BR}(B^0 \to K^{*0}\gamma)$	$4.22 \pm 0.34 \pm 0.85 \pm 0.30$	4.33 ± 0.18
$10^4 \times \mathrm{BR}(B^+ \to K^{*+}\gamma)$	$4.42 \pm 0.36 \pm 0.90 \pm 0.32$	4.21 ± 0.15

Table 8: SM predictions and experimental world averages for the branching ratios of $B^0 \to K^{*0}\gamma$ and $B^+ \to K^{*+}\gamma$. The theory uncertainty is split into parametric, form factor, and non-factorisable power correction uncertainties.

with a form factor measurement. The $B \to (\rho, \omega)\ell\nu$ decays, discussed in section 3.5, are more favourable in this respect.

Another cross-check is the branching ratio of the decay $B \to K^* e^+ e^-$ at very low q^2 that is dominated by the photon pole and that has been measured recently by LHCb [61],

$$\mathrm{BR}(B \to K^* e^+ e^-)^{30\text{–}1000\,\mathrm{MeV}}_{\mathrm{exp}} = (3.1^{+0.9+0.2}_{-0.8-0.3} \pm 0.2) \times 10^{-7}, \tag{30}$$

where the superscript refers to $\sqrt{q^2}$. An interesting observable is the ratio of this branching ratio to the $B \to K^*\gamma$ branching ratio, since theoretical uncertainties, factorisable and or non-factorisable, cancel to a high degree. In the SM, we predict

$$R_{ee,\gamma} \equiv \frac{\mathrm{BR}(B^0 \to K^{*0} e^+ e^-)^{30\text{–}1000\,\mathrm{MeV}}}{\mathrm{BR}(B^0 \to K^{*0}\gamma)} = 0.62 \pm 0.03\,, \tag{31}$$

where the residual error is dominated by form factor uncertainties. Combining experimental errors in quadrature, from the LHCb measurement and the world average of $\mathrm{BR}(B^0 \to K^{*0}\gamma)$, we obtain

$$R^{\mathrm{exp}}_{ee,\gamma} = 0.72 \pm 0.21 \tag{32}$$

which is consistent with the prediction, albeit with sizeable uncertainties. Finally, for the angular observable F_L, that has been measured recently in $B^0 \to K^* e^+ e^-$ at low q^2 [62], we predict

$$F_L(B \to K^* e^+ e^-)^{20\text{–}1000\,\mathrm{MeV}} = 0.109 \pm 0.004 \pm 0.027 \pm 0.008\,. \tag{33}$$

This is in very good agreement with the experimental value,

$$F_L(B \to K^* e^+ e^-)^{20\text{–}1000\,\mathrm{MeV}}_{\mathrm{exp}} = 0.16 \pm 0.06 \pm 0.03\,. \tag{34}$$

3.3. $B_s \to \phi\mu^+\mu^-$ at low q^2

The decay channel $B_s \to \phi\mu^+\mu^-$ is based on the same quark level transition as $B \to K^*\mu^+\mu^-$ and may serve to contrast possible deviations. An important difference between the two channels is that the ϕ-meson decays to K^+K^-, implying that the decay is not self-tagging in contrast to $B_d \to K^*\mu^+\mu^-$, where the flavour of the initial B-meson can be inferred from the charge of the $K\pi$ decay products of the K^*. As a consequence, among the observables discussed for $B \to K^*\mu^+\mu^-$, A_{FB} and S_5 cannot be measured at a hadron collider.

Other than CP asymmetries, the most interesting observables are then the differential branching ratio, F_L, and S_4, in the SM and beyond. For these observables, the three possible sources of difference between the results for $B_s \to \phi\mu^+\mu^-$ and those for $B \to K^*\mu^+\mu^-$ are as follows,

$B_s \to \phi\mu^+\mu^-$		
Observable	q^2 bin	SM prediction
$10^7 \, \frac{d\mathrm{BR}}{dq^2}$	$[0.1, 1]$	$1.221 \pm 0.083 \pm 0.140 \pm 0.060$
	$[1, 2]$	$0.589 \pm 0.035 \pm 0.074 \pm 0.019$
	$[2, 3]$	$0.531 \pm 0.031 \pm 0.070 \pm 0.018$
	$[3, 4]$	$0.536 \pm 0.032 \pm 0.070 \pm 0.021$
	$[4, 5]$	$0.561 \pm 0.035 \pm 0.071 \pm 0.026$
	$[5, 6]$	$0.597 \pm 0.041 \pm 0.073 \pm 0.032$
	$[1.1, 2.5]$	$0.564 \pm 0.072 \pm 0.072 \pm 0.018$
	$[2.5, 4]$	$0.533 \pm 0.070 \pm 0.070 \pm 0.020$
	$[4, 6]$	$0.579 \pm 0.071 \pm 0.071 \pm 0.029$
F_L	$[0.1, 1]$	$0.324 \pm 0.010 \pm 0.042 \pm 0.017$
	$[1, 2]$	$0.751 \pm 0.007 \pm 0.032 \pm 0.018$
	$[2, 3]$	$0.837 \pm 0.002 \pm 0.021 \pm 0.009$
	$[3, 4]$	$0.824 \pm 0.002 \pm 0.022 \pm 0.007$
	$[4, 5]$	$0.779 \pm 0.003 \pm 0.026 \pm 0.013$
	$[5, 6]$	$0.726 \pm 0.004 \pm 0.030 \pm 0.020$
	$[1.1, 2.5]$	$0.787 \pm 0.028 \pm 0.028 \pm 0.016$
	$[2.5, 4]$	$0.829 \pm 0.021 \pm 0.021 \pm 0.006$
	$[4, 6]$	$0.752 \pm 0.028 \pm 0.028 \pm 0.016$
S_4	$[0.1, 1]$	$0.098 \pm 0.001 \pm 0.002 \pm 0.002$
	$[1, 2]$	$0.019 \pm 0.004 \pm 0.008 \pm 0.009$
	$[2, 3]$	$-0.085 \pm 0.004 \pm 0.010 \pm 0.012$
	$[3, 4]$	$-0.155 \pm 0.003 \pm 0.012 \pm 0.013$
	$[4, 5]$	$-0.201 \pm 0.002 \pm 0.013 \pm 0.013$
	$[5, 6]$	$-0.231 \pm 0.001 \pm 0.012 \pm 0.011$
	$[1.1, 2.5]$	$-0.013 \pm 0.008 \pm 0.008 \pm 0.010$
	$[2.5, 4]$	$-0.139 \pm 0.012 \pm 0.012 \pm 0.013$
	$[4, 6]$	$-0.217 \pm 0.012 \pm 0.012 \pm 0.012$
P_4'	$[0.1, 1]$	$0.252 \pm 0.003 \pm 0.005 \pm 0.006$
	$[1, 2]$	$0.048 \pm 0.010 \pm 0.019 \pm 0.022$
	$[2, 3]$	$-0.248 \pm 0.012 \pm 0.028 \pm 0.041$
	$[3, 4]$	$-0.426 \pm 0.006 \pm 0.021 \pm 0.033$
	$[4, 5]$	$-0.498 \pm 0.003 \pm 0.016 \pm 0.022$
	$[5, 6]$	$-0.528 \pm 0.002 \pm 0.013 \pm 0.015$
	$[1.1, 2.5]$	$-0.035 \pm 0.023 \pm 0.023 \pm 0.029$
	$[2.5, 4]$	$-0.389 \pm 0.023 \pm 0.023 \pm 0.036$
	$[4, 6]$	$-0.512 \pm 0.014 \pm 0.014 \pm 0.018$

Table 9: Standard model predictions for binned $B_s \to \phi\mu^+\mu^-$ observables, where the uncertainties are split into parametric uncertainties, form factor uncertainties, and our estimate of the uncertainties due to missing hadronic effects.

- the form factors are different;
- differences induced by spectator effects, e.g. weak annihilation;
- effects due to the sizeable B_s-$\bar{B}_s$ lifetime difference.

The form factors have already been discussed in secs. 2.5 and 2.6. The spectator effects turn out to be very small in the SM and are not relevant compared to the form factor uncertainties. For a discussion of effect beyond the SM we refer the reader to the appendix of ref. [7]. The lifetime effects stems from the fact that, in contrast to B_d mesons, the lifetimes of B_s and $\bar{B}_s$ differ by roughly 8%. This leads to a difference between the observables defined in the absence of neutral meson oscillations, as used in the case of $B_d \to K^*\mu^+\mu^-$, and time-integrated observables, as measured experimentally. This difference has to be taken into account when comparing theory predictions to experimental data. In appendix E, we show that this effect can have a sizeable impact on the $B_s \to \phi\mu^+\mu^-$ observables in the presence of non-standard CP violation. In the SM, however, it turns out that the effect is negligible.

In table 9, we list our numerical predictions for the differential branching ratio and angular observables accessible from an untagged measurement $B_s \to \phi\mu^+\mu^-$. The uncertainties are treated in the same way as for $B \to K^*\mu^+\mu^-$.

3.4. $R_{K^*\phi}$: $B \to K^*\mu^+\mu^-$ versus $B_s \to \phi\mu^+\mu^-$

The similarity of the $B \to K^*\mu^+\mu^-$ and $B_s \to \phi\mu^+\mu^-$ channels implies that the uncertainties of ratios of these observables should be strongly reduced.[13] Theory predicts $B_s \to \phi\mu^+\mu^-$ to have a higher transition than $B \to K^*\mu^+\mu^-$ which essentially comes from the decay constants (c.f. tab. 1)showing this hierarchy. At low q^2 and for $\phi(K^*)\gamma$ final state (i.e. $q^2 = 0$) the central values of the LHCb results show the opposite effect.

First, we recapitulate the prediction for the branching ratio of $B_s \to \phi\gamma$ (see appendix A of ref. [7] for more details) versus $B \to K^*\gamma$. The effect is driven by $T_1^{B\to K^*}(0)/T_1^{B_s\to\phi}(0) = 0.89 \pm 0.10$[14] which mainly results from the above mentioned decay constants

$$R^{(\gamma)}_{K^*\phi} = \frac{\mathrm{BR}(B^0 \to K^{*0}\gamma)}{\mathrm{BR}(B_s \to \phi\gamma)} = 0.78 \pm 0.18\,, \tag{35}$$

which is roughly 1.5 standard deviations below the LHCb measurement for this ratio, 1.23 ± 0.32 [63]. Such a deviation can, of course, not be regarded as statistically significant.

A similar ratio can also be considered for the decay to leptons,

$$R_{K^*\phi}[q_1, q_2] \equiv \frac{d\mathrm{BR}(B^0 \to K^{*0}\ell^+\ell^-)/dq^2|_{[q_1,q_2]}}{d\mathrm{BR}(B_s \to \phi\ell^+\ell^-)/dq^2|_{[q_1,q_2]}}, \tag{36}$$

by considering ratios of the differential branching ratios integrated over specified ranges in q^2. We show a graphical comparison of our predictions using LCSR, lattice and combinations of the two for the ratio $R_{\phi K^*}$ to the results of LHCb [40, 64] and CDF [65] at both low and high q^2 in fig. 3. Again, rhe results per se are not statistically significant. On the qualitative level it is though interesting that the theoretical and the experimental ratio are below and above

[13] In this work we have not performed an error analysis on the ratios themselves. The latter would greatly reduce the error and could be undertaken if the experimental central values persist with smaller uncertainties.

[14] The central value of this work, which is a more complete update, is $T_1^{B\to K^*}(0)/T_1^{B_s\to\phi}(0) = 0.93$.

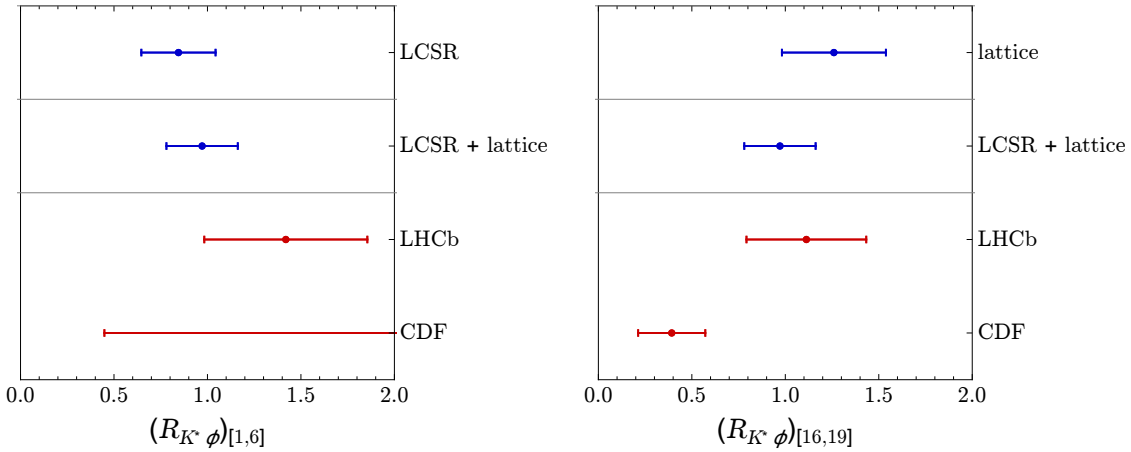

Figure 3: Our predictions for $R_{\phi K^*}$ at low and high q^2 using LCSR, Lattice and a combination of the two, compared to experimental results from LHCb [40, 64] and CDF [65].

unity respectively. It is hard to see how the theoretical value can move above one, through redetermination of parameters, without uncovering a new physical effect. We stress once more that we have not undertaken an analysis with correlated errors for this quantity. Once could easily expect the theory error to do down by a factor of two by doing so which would result in $R_{K^*\phi}|_{[1,6]} < 1$ within uncertainties. We are looking forward to the 3fb^{-1} results to reexamine this issue.

3.5. $|V_{\rm ub}|$ from $B \to (\rho, \omega)\ell\nu$

FCNC decays such as $B \to K^*\mu^+\mu^-$ and $B_s \to \phi\mu^+\mu^-$ are potentially affected by new physics they do not provide a clean environment to test form factor predictions. The semi-leptonic charged current $B^{0,+} \to (\omega, \rho^{-,0})\ell^+\nu$ occur at tree-level, and is therefore less likely to be affected by new physics and serves to test form factor predictions. In particular in view of the current discrepancies between the $B \to K^*\mu^+\mu^-$ and $B_s \to \phi\mu^+\mu^-$ branching fraction measurements the normalisation of the form factors per se has become an issue of considerable interest.

The differential branching ratios of these decays, for $m_\ell = 0$, are given by

$$\frac{d\text{BR}(B^0 \to \rho^-\ell^+\nu)}{dq^2} = \tau_{B^0}|V_{\rm ub}|^2 \frac{G_F^2}{192\pi^3 m_B^3}\sqrt{\lambda}\left(|\mathcal{V}^{(+)}|^2 + |\mathcal{V}^{(-)}|^2 + |\mathcal{V}^{(0)}|^2\right), \tag{37}$$

$$\frac{d\text{BR}(B^+ \to \rho^0\ell^+\nu)}{dq^2} = \frac{\tau_{B^+}}{2\tau_{B^0}}\frac{d\text{BR}(B^0 \to \rho^-\ell^+\nu)}{dq^2}, \tag{38}$$

where definitions of $\mathcal{V}^{(\iota)}$ for $\iota = +, -, 0$ as well as λ, the Källén-function, can be found in appendix B, with the adaption $m_{K^*} \to m_\rho$. The one for $B^+ \to \omega\ell^+\nu$ is analoguous to $B^+ \to \rho^0\ell^+\nu$ with obvious replacements.

The most recent measurements of the branching ratios have been performed for $B \to \rho\ell\nu$ by BaBar [66] and Belle [67] and for $B \to \omega\ell\nu$ by BaBar [68, 69] and Belle [67] respectively. We extract $|V_{\rm ub}|$ from the BaBar and Belle data by minimizing the χ^2 function that reads in both cases

$$\chi^2(|V_{\rm ub}|) = \sum_{ij} \left[B^i_{\rm exp} - B^i_{\rm th}(|V_{\rm ub}|)\right] (C^{ij}_{\rm exp} + C^{ij}_{\rm th})^{-1} \left[B^j_{\rm exp} - B^j_{\rm th}(|V_{\rm ub}|)\right] , \tag{39}$$

where $B^i_{\rm exp}$ and $B^i_{\rm th}$ are the experimental and theoretical central values for the branching ratios in one q^2-bin and the sum runs over all bins for the charged and neutral mode. $C_{\rm th}$ is the theoretical covariance matrix that includes in particular the correlated form factor uncertainties. In the case of Belle, we use the data up to $q^2 = 8\,{\rm GeV}^2$ or $12\,{\rm GeV}^2$ and take the full covariance matrix provided in ref. [67]. The BaBar dataset consists of a single bin in the low-q^2 region from 0 to 8 GeV^2 and the correlation between the charged and neutral decay is not provided. For $B \to \rho\ell\nu$ we obtain

$$|V_{\rm ub}|^{B\to\rho\ell\nu}_{\text{Belle, } q^2<8{\rm GeV}^2} = (3.45 \pm 0.12 \pm 0.24) \times 10^{-3} , \tag{40}$$

$$|V_{\rm ub}|^{B\to\rho\ell\nu}_{\text{Belle, } q^2<12{\rm GeV}^2} = (3.29 \pm 0.09 \pm 0.20) \times 10^{-3} , \tag{41}$$

$$|V_{\rm ub}|^{B\to\rho\ell\nu}_{\text{BaBar, } q^2<8{\rm GeV}^2} = (2.54 \pm 0.29 \pm 0.15) \times 10^{-3} , \tag{42}$$

and those from $B^+ \to \omega\ell^+\nu$ we get

$$|V_{\rm ub}|^{B\to\omega\ell\nu}_{\text{Belle, } q^2<7{\rm GeV}^2} = (2.54 \pm 0.35 \pm 0.24) \times 10^{-3} , \tag{43}$$

$$|V_{\rm ub}|^{B\to\omega\ell\nu}_{\text{BaBar, } q^2<8{\rm GeV}^2} = (3.33 \pm 0.25 \pm 0.32) \times 10^{-3} , \tag{44}$$

$$|V_{\rm ub}|^{B\to\omega\ell\nu}_{\text{BaBar, } q^2<12{\rm GeV}^2} = (3.31 \pm 0.19 \pm 0.30) \times 10^{-3} , \tag{45}$$

where the first error is experimental and the second theoretical.

Our results can be compared to the value extracted from $B \to \pi\ell\nu$ decays, obtained in ref. [67] from a global fit of BaBar and Belle data to lattice and LCSR computations,

$$|V_{\rm ub}|^{B\to\pi\ell\nu} = (3.41 \pm 0.22) \times 10^{-3} , \tag{46}$$

or the average of the inclusive semi-leptonic $b \to u$ determinations [33]

$$|V_{\rm ub}|^{\rm incl.} = 4.41(15)(^{15}_{17}) \times 10^{-3} , \tag{47}$$

where the first error is experimental and the second error is theoretical. Finally we also compare our results to the values obtained indirectly from global fits of the CKM matrix [70, 71],

$$|V_{\rm ub}|_{\rm CKMfitter} = (3.44^{+0.25}_{-0.08}) \times 10^{-3} , \qquad |V_{\rm ub}|_{\rm UTfit} = (3.61 \pm 0.12) \times 10^{-3} . \tag{48}$$

The various values for $|V_{\rm ub}|$ quoted in this section are summarised graphically in fig. 4.

The $B \to (\rho, \omega)$ form factors do not, and should not, incorporate an S-wave contribution since the $(\rho, \omega) \to \pi\pi$ is necessarily in a P-wave (c.f. section 2.3). Hence the experimental branching ratios might be too large which in turn leads to a systematic upward shift of $|V_{\rm ub}|$ as extracted from these analyses. In ref. [27] (c.f. fig. 9 of that reference) this effect has been analysed and it has been found that the integrated line shapes of the S-wave over the interval $[m_\rho - \Gamma_\rho, m_\rho + \Gamma_\rho]$ is around 12% of the corresponding P-wave contribution. This means that

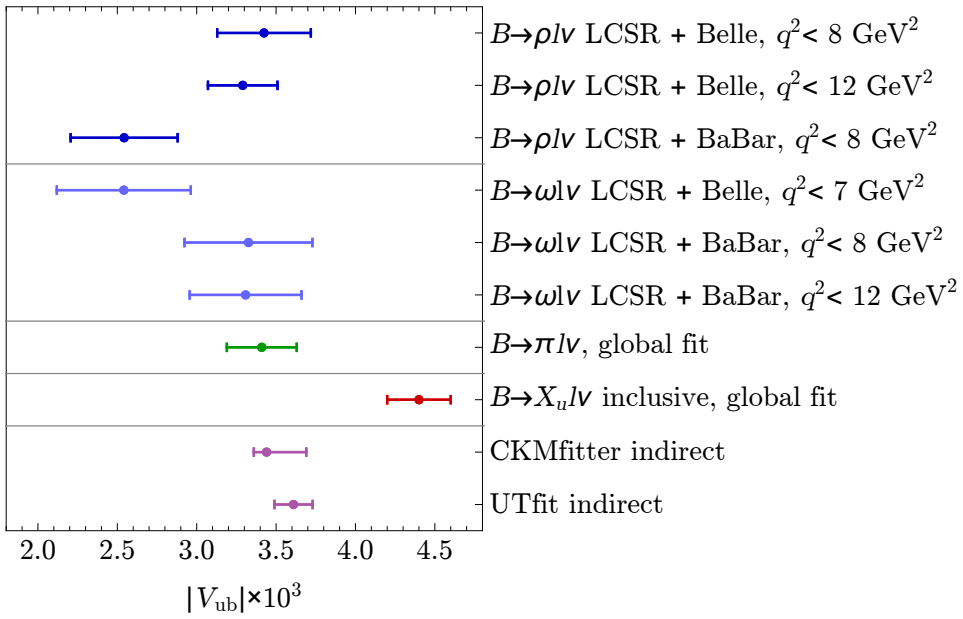

Figure 4: Our predictions for $|V_{ub}|$ from $B \to \rho\ell\nu$ and $B \to \omega\ell\nu$ (blue) compared to global fits to V_{ub} from exclusive [33] and inclusive channels [67] and indirect determinations from fits of the unitarity triangle [70, 71].

if the S-wave is neglected altogether then we can expect an upward shift of $\sim 6\%$ of the $|V_{ub}|$ values. In the BaBar and Belle analysis the S-wave has not been subtracted systematically. Hence if the precision below the 10%-level is to be reached then the experimental analyses has to perform an angular analysis[15] in order to subtract the S-wave.

Leaving aside the inclusive determinations we conclude that our $|V_{ub}|$-values from the combined Belle & BaBar analysis are somewhat lower but surely consistent with $B \to \pi\ell\nu$ determinations as well as the global CKM fits. The values of $|V_{ub}|$ which are considerably lower than the average come with large experimental uncertainties and are consistent at the level of one standard deviation. The uncertainty is rather large and an updated analysis with the full BaBar data set will be more telling.

4. Conclusions

In this paper we present an update of the light-cone sum rules form factors relevant for the B to vector transitions $B_{d,s} \to K^*, \rho, \omega, \phi$ using current hadronic input. To corroborate the robustness of our predictions, we have discussed in detail the role of the equations of motion in reducing the uncertainties of tensor-to-vector form factor ratios and mass scheme dependence in section 2.2 and appendix A.5 respectively. The (non-)impact of the V-mesons being an unstable particle is analysed in section 2.3.

An important point of this work are the easy-to-use numerical expressions of the form factors, provided to the phenomenological community, that allow to retain all the uncertainty correlations among the form factors in phenomenological analyses. This is of particular im-

[15] For the $\pi\pi$ final state one can make use of the isospin in order to deduce whether its an S- or P-wave contribution [23].

portance for predicting angular observables that involve ratios of form factors. We fitted a z-expansion, eq. (15), to the form factors and provide central values, uncertainties, and correlation matrices of the expansion coefficients in electronic form as ancillary files on the arXiv webages (see appendix D for details and table 11 for the central values). The parameterisation is chosen to transparently fulfil the two exact relations among the form factors at $q^2 = 0$. In addition we performed combined fits to LCSR and lattice computations of the form factors. This serves on the one hand to obtain predictions for the form factors valid in the full kinematic range, on the other hand as a cross-check of the consistency between the two complementary approaches, as they have to coincide for intermediate q^2 values. Good agreement is observed with the exception of the form factor T_{23}. The latter however plays a negligible role in $B \to V\ell^+\ell^-$ observables. Likewise the z-expansion coefficients and the correlated uncertainties of the combined fits are as downloadable files (and central values in table 12).

A phenomenological analysis is performed using the updated predictions and a new treatment of theoretical uncertainties. In sections 3.1 and 3.2, we have given updated Standard Model predictions for $B \to K^*\mu^+\mu^-$ and $B \to K^*\gamma$ observables, taking into account LCSR calculations of several hadronic effects beyond form factors and a conservative estimate of the uncertainties due to missing hadronic effects, notably contributions from charm quarks. Likewise, in section 3.3 we have given predictions for $B_s \to \phi\mu^+\mu^-$ observables, showing (in appendix E) that the effect of the finite B_s-lifetime difference is negligible in the Standard Model. Our predictions are particularly relevant in view of several apparent tensions between Standard Model expectations and experimental measurements observed recently. A crucial question to address in the near future will be whether these tensions are due to underestimated hadronic effects or physics beyond the Standard Model. Our improved form factor predictions can play an important role in answering this question.

In section 3.5, the new form factor predictions were used to extract the CKM element $|V_{\rm ub}|$ from BaBar and Belle measurements of $B \to (\rho,\omega)\ell\nu$ decays. Barring some disagreement among the experiments, we find good agreement of our predictions with other exclusive predictions, e.g. $B \to \pi\ell\nu$ and global fits. Our results contribute to the enhancement of the ongoing tension between the exclusive and inclusive determination of $|V_{\rm ub}|$. From another viewpoint the encouraging agreement with other exclusive channels serve as a test of the form factor normalisation which might become particularly important if the disagreement of $B \to K^*\ell^+\ell^-$ versus $B_s \to \phi\ell^+\ell^-$ becomes more significant. Our predictions for $|V_{\rm ub}|$ have a relative theory uncertainty at the level of 6-7% from $B \to \rho$ and 9-10% from $B \to \omega$, showing the potential of future, more precise measurements of these semi-leptonic decays to improve the precision on $|V_{\rm ub}|$.

We conclude by emphasising that our improved form factor predictions are important for the tensions in both $b \to s$ channels and the determination of $|V_{\rm ub}|$. These questions can be further examined with future experimental data to which we look forward to.

Acknowledgments

We thank Wolfgang Altmannshofer, Martin Beneke, Christoph Bobeth, Vladimir Braun, Gerhard Buchalla, Gilberto Colangelo, Greig Cowan, Jochen Dingfelder, Thorsten Feldmann, Gudrun Hiller, Lars Hofer, Fred Jegerlehner, Vera Luth, Stefan Meinel, Steve Playfer, Christoph Schwanda, Peter Stoffer and Yuming Wang for useful discussions. R.Z. is particularly grateful to Patricia Ball for collaboration on $B \to V$ form factor computations in the past. The research of D.S. is supported by the DFG cluster of excellence "Origin and Structure of the Universe".

A. Relevant aspects of the LCSR determination of the form factors

A.1. Equation of motion and correlation functions

The LCSR form factors are computed from a correlation function of the type

$$C[\Gamma] = i \int d^4x e^{ip_B x} \langle K^*(p)|T\{\bar{s}\Gamma b(0) J_B(x)\}|0\rangle \ , \tag{A.1}$$

where Γ is the Dirac-structure and $J_B \equiv m_b \bar{b} i\gamma_5 q$ an interpolating field for the B-meson. In fact the projection on the B-meson through a dispersion relation and the Borel transformation can be seen as the substitute of the LSZ-formalism for the B-meson. The eom (5) inserted into such correlation functions hold up to contact terms, denoted by $\Delta_\mu^{(5)}$,

$$q^\nu C[i\sigma_{\mu\nu}(\gamma_5)] + \Delta_\mu^{(5)} = -(m_s \pm m_b) C[\gamma_\mu(\gamma_5)] + C[i(\overleftarrow{\partial} + \overrightarrow{\partial})_\mu(\gamma_5)] - 2iC[\overleftarrow{D}_\mu\ (\gamma_5)] \ . \tag{A.2}$$

A heuristic derivation of the contact term follows from the time derivative acting on the time ordering of the operators which leads to a commutator expression

$$\Delta_\mu^{(5)} = -\int d^3x e^{-i\vec{p_B}\cdot\vec{x}} \langle K^*(p,\eta)|[\bar{s} i\sigma_{\mu 0}(\gamma_5) b(0), J_B(\vec{x},0)]|0\rangle \ . \tag{A.3}$$

Using the canonical equal-time commutation relation for the b-quarks, $\{b_\alpha^\dagger(\vec{x},0), b_\beta(0)\} = \delta^{(3)}(\vec{x})\delta_{\alpha\beta}$, leads to[16]

$$\Delta_\mu = 0 \text{ and } \Delta_\mu^5 = -im_b f_V \eta_\mu^* \ . \tag{A.4}$$

The crucial point is that the contact term is a local term which does not affect the extraction of the form factors at all since it does not enter the dispersion relation. Hence the form factors which are determined from the correlation function in LCSR obey the eom. More precisely the eom impose constraints or correlations on Borel parameters and continuum thresholds of sum rule parameters.

A.2. Correlation of continuum thresholds and Borel parameters

Each correlation function obeys a dispersion relation. Using the notation $C[\gamma^\mu] = C_1[\gamma^\mu]P_1^\mu + ..$, $C_1[\gamma^\mu]$ can be written as

$$C_1[\gamma^\mu] = \int_{\text{cut}}^\infty ds \frac{\rho_1[\gamma^\mu](s)}{s - p_B^2 - i0} = \frac{m_B^2 \mathcal{V}_1(q^2) f_B}{p_B^2 - m_B^2} + \int_{s_c}^\infty ds \frac{\rho_1[\gamma^\mu](s)}{s - p_B^2 - i0} \ , \tag{A.5}$$

where s_c marks the continuum threshold and cut stands for the beginning of the discontinuity which is just below $p_B^2 = m_B^2$. Since (A.2) is valid for any p_B^2 it follow from the representation (A.5) that the equations of motion are valid for the densities $\rho_1(s)$ point by point, i.e. locally. In particular subtracting the form factor eom (6) from (A.2) we obtain

$$q^\nu \int_{s_c}^\infty ds \frac{\rho_1[i\sigma_{\mu\nu}(\gamma_5)](s)}{s - p_B^2 - i0} = -(m_s + m_b) \int_{s_c}^\infty ds \frac{\rho_1[\gamma^\mu](s)}{s - p_B^2 - i0} - 2i \int_{s_c}^\infty ds \frac{\rho_1[\overleftarrow{D}_\mu](s)}{s - p_B^2 - i0} \tag{A.6}$$

[16] In the computation we have assumed that the vector meson is at rest. The result (A.4) is the covariantised version. Alternatively we could have derived the contact term directly from the path integral through field transformations or the (covariant) T^*-product. Both of which should directly yield a covariant result.

for the direction P_1^μ with a somewhat elaborate notation. This is of course true for the exact density as well as for the density $\rho_1^{\text{LC-OPE}}$ computed from the light-cone OPE. The semi-global quark-hadron duality, or sum rule approximation, consists of replacing the integral on the right-hand side of (A.5) by:

$$\int_{s_c}^{\infty} ds \frac{\rho_1(s)}{s - p_B^2 - i0} \simeq \int_{s_0^V}^{\infty} ds \frac{\rho_1^{\text{LC-OPE}}(s)}{s - p_B^2 - i0} \,, \tag{A.7}$$

where s_0^V is some effective threshold parameter which is expected to lie somewhere between $(m_B + 2m_\pi) \simeq 30.9\,\text{GeV}^2$ and $(m_B + m_\rho)^2 = 36.6\,\text{GeV}^2$. A simple way to achieve consistency with the eom (A.2) is to impose $s_0^V = s_0^{T_1} = s_0^{\mathcal{D}_1}$. From a physical perspective this is a natural choice since the currents have got the same quantum numbers and therefore the same spectrum of states coupling to it. We argue that the eom strengthen this point implying a high degree of correlation of the continuum thresholds.

Our main point is that since $\mathcal{D}_1 \ll T_1, V$, which we infer from the closeness of $r_\perp$ (11) to unity (c.f. fig. 1), a relative difference between s_0^V and $s_0^{T_1}$ can only be compensated by a much larger change in $s_0^{\mathcal{D}_1}$. The latter corresponds to a gross violation of semi-global quark hadron duality which we exclude; partly on grounds of past experience with LCSR.

More precisely let us choose $r_\perp(0) \simeq 0.937$ which is one of the largest deviations in fig. 1.[17] For example for $s_0^V = 35\,\text{GeV}^2$ and $s_0^{T_1} = s_0^V \pm 1\,\text{GeV}^2$, with fixed Borel parameters, the eom (6) requires $s_0^{\mathcal{D}_1} = 35\,\binom{+15}{-6.5}\,\text{GeV}^2$ which are considerable, not to say absurd, shifts. This corresponds to a change in the form factor $\mathcal{D}_1$ of $+55\%$ and -63% respectively. From this we infer that a difference of $1\,\text{GeV}^2$ on the two continuum thresholds $s_0^{T_1} - s_0^V$ is at the upper boundary of what seems plausible. For $s_0^{T_1,V} = 35(2)\,\text{GeV}^2$ this can be imposed by correlating the two form factors by 7/8 (i.e. 87.5%). The same line of reasoning applies to $r_\parallel$ and r_{0+t} (11). Yet for r_{0+t} the numerics are less compelling and we restrict the correlation between to 50%. There are two further correlations at $q^2 = 0$, namely $T_1(0) = T_2(0)$ which is of the algebraic type and $A_0(0) = A_3(0)$ which is required to avoid an unphysical pole at $q^2 = 0$. This leads to $s_0^{T_1} = s_0^{T_2}$ and $s_0^{\mathcal{V}_0} = s_0^{A_0}$. Strictly speaking the latter two are only exact at $q^2 = 0$ but since we refrain from assigning a q^2-dependence to s_0 the relation is assumed throughout.

In summary we get the following correlations:

$$\text{corr}(s_0^{T_1}, s_0^V) = 7/8 \,, \quad \text{corr}(s_0^{T_2}, s_0^{A_1}) = 7/8 \,, \quad \text{corr}(s_0^{A_{12}}, s_0^{T_{23}}) = 1/2 \,, \tag{A.8}$$

and the full correlations $\text{corr}(s_0^{T_1}, s_0^{T_2}) = 1$ and $\text{corr}(s_0^{A_0}, s_0^{A_{12}}) = 1$ together with (A.8) imply

$$\text{corr}(s_0^{T_1}, s_0^{A_1}) = 7/8 \,, \quad \text{corr}(s_0^{T_2}, s_0^V) = 7/8 \,, \quad \text{corr}(s_0^{A_{12}}, s_0^{A_0}) = 1/2 \,. \tag{A.9}$$

We remind the reader that we have argued in section 2.4 for a correlation of the type $\text{corr}(s_0^F, s_0^{f_B}) = 1/2$ where F stands for any form factor and $s_0^{f_B}$ is the continuum threshold for the f_B sum rule.

So far we have not discussed the role of the Borel parameter. In principle one could argue that the Borel parameter and the continuum threshold can conspire to satisfy the eom. Whereas this does not seem to be very viable from the point of view of physics it is in addition not

[17] The main conclusions remain unchanged when other points are chosen. For example $r_\parallel(6\,\text{GeV}^2) \simeq 0.990$ requires shifts of $s_0^{\mathcal{D}_1} = 35\,\binom{+16}{-7.7}\,\text{GeV}^2$ for $s_0^{T_2} = 35 \pm 1\,\text{GeV}^2$ and changes the ratio of T_2 to A_1 by 3%. The difference to the case discussed below is that the relative change in $\mathcal{D}_2$ is larger due to the accidental closeness of $\mathcal{D}_2$ to unity as compared to that of $\mathcal{D}_1$.

credible on grounds of the actual numerics. For example doubling the Borel parameter of the light-cone sum rule $M^2_{\rm LC}$, keeping the Borel parameter $M^2_{f_B}$ of the f_B sum rule fixed, leads to a change in the form factors T_1 and V of just one percent. Doubling the sum rule parameter is outside the validity range since it enhances the continuum contributions relative to the B-pole contribution. For example for $T_1(0)$ the continuum contribution becomes 42% by doubling $M^2_{\rm LC}$. Hence the Borel parameter cannot balance a change in the continuum threshold of s_0 of $1{\rm GeV}^2$. Hence it is legitimate not to enter the $M^2_{\rm LC}$ in the discussion. The sensitivity of the f_B sum rule to the Borel parameter $M^2_{f_B}$ is slightly higher presumably because the local condensates are more vulnerable to quark hadron duality violations. This uncertainty is important for the form factor prediction per se but only enters the eom by a global factor and is therefore not relevant for the discussion of this section. We fully correlate the uncertainties of the Borel parameters ${\rm corr}(M^2_{f_B}, M^2_F) = 1$ which is justified since the variation in s_0 are responsible for the uncertainty. In practice both M^2 and s_0 do assess the validity of the semi-global quark hadron duality.

A.3. Remarks on the explicit verification of the eom at tree level

In view of the importance of the eom in the determination of the ratio of tensor to vector form factors discussed in the previous section, we intend to give some more details on the explicit verification of eq. 5.

We have explicitly verified the eom at tree level up to twist 3 by computing all five structures appearing in (A.2) which in particular includes the derivative form factors. More precisely we have incorporated the DA $\phi_{\perp,\parallel}$ and $g^{\perp}_{v,a}$ whose definitions can be found in [7, 12] for instance. Not surprisingly the eom are found to be obeyed upon using the eom of the DA. Explicit results are given in the next subsection A.4. Let us hasten to add that according to taste one might find it convenient to use the identity,

$$C[i(\overleftarrow{\partial} + \overrightarrow{\partial})_\mu] - 2iC[\overleftarrow{D}_\mu] = -C[i(\overleftarrow{\partial} + \overrightarrow{\partial})_\mu] + 2iC[\overrightarrow{D}_\mu] \tag{A.10}$$

which allows one to interchange the action of the covariant derivative between the strange and beauty quark.

To this end we would like to discuss the consistent handling of the projection onto the structures P^μ_i (2). First, we note that for the eom to be satisfied the projection on the Lorentz structures ought to be handled consistently for all structures appearing in (A.2). For $P^\mu_{2,3}$ extra care is in order, see e.g. discussion in [53], since $q\cdot(p+p_B) = p_B^2 - m_V^2$ equals $m_B^2 - m_V^2$ only if p_B^2 is on-shell. Hence in the computation the following projectors ought to be used

$$\begin{aligned} p^\mu_2 &= i\{q\cdot(p+p_B)\eta^{*\mu} - (\eta^*\cdot q)(p+p_B)^\mu\}\,, \\ p^\mu_3 &= i(\eta^*\cdot q)\{q^\mu - \frac{q^2}{q\cdot(p+p_B)}(p+p_B)^\mu\}\,, \end{aligned} \tag{A.11}$$

which we denote by a lower case p. The important point is that these projectors are transverse $q\cdot p_i = 0$ in the off-shell case. We should add that the actual effect on the standard tensor and vector form factors due to the use of $p^\mu_{2,3}$ or $P^\mu_{2,3}$ is rather small (numerically around 2%) since the the sum rule assures by construction that $p_B^2 \simeq m_B^2$. The latter might be taken as a measure of the quality of the sum rule. See also the discussion on the optimisation of the Borel parameter given in appendix A.6.

A.4. Explicit tree level results

Let us parameterise a generic form factor by

$$F(q^2) = \frac{m_b}{m_B^2 f_B}\int_{u_0^F}^1 e^{(m_B^2-(m_b^2-\bar{u}q^2)/u)/M_F^2}\bar{\rho}_F(u,q^2)du\ , \tag{A.12}$$

where $u_0^F \equiv (m_b^2-q^2)/(s_0^F-q^2)$ with s_0 the continuum threshold parameter and M_F^2 the Borel parameter. We find that the explicit results at tree-level up to twist 3 $O(m_V)$ are given by

$$\begin{aligned}
\bar{\rho}_{A_0} &= \frac{1}{2u}m_b f_V(g_v^\perp(u)+\Phi(u)') + .. \ , \\
\bar{\rho}_{T_1} &= \frac{1}{8u}\Big(4f_V^\perp m_b\phi^\perp(u) + f_V m_V(4\Phi(u)+\tilde{g}_a^\perp(u)-\Omega_2 u\tilde{g}_a^\perp(u)'+4ug_v^\perp(u))\Big) + .. \ , \\
\bar{\rho}_V &= (m_B+m_V)\frac{1}{4u}\left(2f_V^\perp\phi^\perp(u) - \frac{f_V m_b m_V}{m_b^2-q^2}u\tilde{g}_a^\perp(u)'\right) + .. \ , \\
\bar{\rho}_{T_2} &= \frac{1}{8u\Omega_u}\Big(4f_V^\perp m_b\phi^\perp(u) + m_V f_V(4\Phi(u)+\tilde{g}_a^\perp(u)-u\tilde{g}_a^\perp(u)'+4\Omega_2 ug_v^\perp(u))\Big) + .. \ , \\
\bar{\rho}_{A_1} &= \frac{(m_B-m_V)}{2u(m_b^2-\bar{u}q^2)}(f_V^\perp(m_b^2-q^2)\phi^\perp(u) + 2f_V m_b m_V u g_v^\perp(u)) + .. \ , \\
\bar{\rho}_{T_3} &= \frac{1}{8u}\Big(m_V f_V(4\Phi(u)+\tilde{g}_a^\perp(u)-u\tilde{g}_a^\perp(u)'+4(u-2)g_v^\perp(u)-8\Omega_u\Phi(u)' + \\
&\qquad 4f_V^\perp m_b\phi^\perp(u))\Big) + .. \\
\bar{\rho}_{A_3} &= \frac{1}{2u}\left(m_b f_V(g_v^\perp(u)+\Omega_u\Phi(u)') - \frac{q^2}{2m_V}f_V^\perp\phi^\perp(u)\right) + .. \ ,
\end{aligned} \tag{A.13}$$

where

$$\Omega_u = \frac{m_b^2-\bar{u}q^2}{m_b^2-q^2}\ , \quad \Omega_2 = \frac{m_b^2+q^2}{m_b^2-q^2}\ . \quad \Phi(u) \equiv \int_0^u(\phi^\parallel(v)-g_v^\perp(v))dv\ .$$

With regard to the eom it is important to emphasise that further m_s dependence enters through $g_a^\perp(u)$ and $g_v^\perp(u)$. In terms of asymptotic twist-2 DA $\phi^\perp(u) = 6\bar{u}u$ and $\phi^\parallel(u) = 6\bar{u}u$ [72]

$$\begin{aligned}
\tilde{g}_a^\perp(u) &= (1-\tilde{\delta}_+)g_a^\perp(u) = 6\bar{u}u + 6\tilde{\delta}_+(2\bar{u}u+\bar{u}\ln\bar{u}+u\ln u) + 6\tilde{\delta}_-(\bar{u}\ln\bar{u}-u\ln u) + .. \ , \\
g_v^\perp(u) &= \frac{3}{4}(1+\xi^2) + \frac{3}{2}\tilde{\delta}_+(2+\ln\bar{u}+\ln u) + \frac{3}{2}\tilde{\delta}_-(2\xi+\ln\bar{u}-\ln u) + .. \ ,
\end{aligned} \tag{A.14}$$

where $\xi \equiv u-\bar{u} = 2u-1$, $\tilde{\delta}_\pm \equiv (m_q \pm m_s)/m_V f_V/f_V^\perp$ and the dots stand for three-particle DA which we have not shown in the densities above. With regard to reference [72] we have introduced the shorthand $\tilde{g}_a^\perp(u) = (1-\tilde{\delta}_+)g_a^\perp(u)$ [18] in order to keep the results in (A.13) compact. We notice that $\rho_{T_1(0)} = \rho_{T_2(0)}$ and $\rho_{A_0(0)} = \rho_{A_3(0)}$ hold as they should. The results for $T_1(0)$, $V(q^2)$ and $A_0(q^2)$ explicitly agree with the expressions given in [51]. The expression for $A_1(q^2)$ differs slightly due to the previously discussed handling of the projections as described in section A.3. In practice the results for each form factor are numerically small but for this

[18] The aim of this redefinition is to keep the normalisation of $g_a^\perp(u)$ simple: $\int_0^1 du g_a^\perp(u) = 1$.

work is of importance since we are interested in a precise determination of the ratio of tensor-to-vector form factor. For example A_1 differs by a prefactor $(m_B^2 - m_V^2)/(q \cdot (p + p_B)) = (m_B^2 - m_V^2)/(p_B^2 - m_V^2) = (m_b^2 - \bar{u}q^2)/(um_B^2) + O(m_V^2)$.

From the results above one can obtain the densities for the derivative form factors. For example for $\mathcal{D}_1$ we obtain

$$\bar{\rho}_{\mathcal{D}_1} = \frac{m_b + m_s}{m_B + m_V}\bar{\rho}_V - \bar{\rho}_{T_1} = \frac{1}{8u}\left(-f_V m_V(4\Phi(u) + \tilde{g}_a^\perp(u) + u\tilde{g}_a^\perp(u)' + 4ug_v^\perp(u))\right) + .. \quad \text{(A.15)}$$

where the $\phi^\perp$-expression exactly cancels.

A.5. Scheme dependence of the form factors

In many determinations of $B \to V, P$ form factor calculation in LCSR the pole mass scheme is assumed to be the appropriate scheme for the b-quark mass. For $B \to \pi$ form factors it has been found that a conversion to the $\overline{\text{MS}}$-scheme leads to minor changes only [34, 73]. The explicit appearance of m_b in the eom (6)-(9) deserves a reinvestigation of the issue of scheme dependence.

In LCSR calculations one distinguishes between a factorisation scale $\mu_F^2 \simeq m_B^2 - m_b^2 \simeq O(m_b\Lambda_{\text{QCD}})$ and a renormalisation scale $\mu_{\text{UV}} = m_b$. The former is the separation scale of the LC-OPE and the latter is the scale of the composite operators e.g. the tensor or vector bilinear quark currents. For the analysis in this appendix and throughout the paper we adopt the strategy to lower μ_{UV} to μ_F in the actual computation and then use renormalisation group running to scale the tensor form factors from $T_i(q^2)|_{\mu_{\text{UV}}=\mu_F}$ to $T_i(q^2)|_{\mu_{\text{UV}}=m_b}$. This makes it clear how the eom are obeyed at any step in the computation. More details on the renormalisation of the composite operators are given in the next subsection.

One can switch back and forth between the pole and $\overline{\text{MS}}$-scheme by replacing $m_b^{\text{pole}} = \bar{m}_b(\mu_m)(1 + \frac{\alpha_s(\mu)}{4\pi}C_F(4 - 3\ln(m_b^2/\mu_m^2)))$ (with $C_F = 4/3$ in QCD) in the tree level computation and expanding to first order in α_s. The additional scale μ_m introduced through the $\overline{\text{MS}}$ scheme shall be set to μ_F for the same reasons as those mentioned above. In table 10 a few examples of form factor determinations in both schemes are given. We infer that the impact of changing from the pole to the $\overline{\text{MS}}$-scheme for the form factors is around 4% which is sizeable but controlled. Yet the ratio of form factors changes by only 1% which is rather small and therefore substantiates one of the main points of this paper. The μ-dependence entering through the μ-dependent $\overline{\text{MS}}$-mass is reflected in the pole scheme through a larger uncertainty in the mass; $m_b^{\text{pole}} = 4.8(1)\,\text{GeV}$ as compared to $\bar{m}(\bar{m}) = 4.18(3)\,\text{GeV}$ [33].

A.5.1. Renormalisation of composite operators

The aim of this section is to clarify the renormalisation of the composite operators entering the eom (5) with particular focus on the m_b quark mass. We introduce the following shorthand notations for the operators

$$\begin{aligned} O_1 &= O_D = 2\bar{s}i\overleftarrow{D}_\mu\, b\,, & O_2 &= O_{\partial T} = i\partial^\nu(\bar{s}i\sigma_{\mu\nu}b)\,, \\ O_3 &= O_{mV} = (m_s + m_b)\bar{s}\gamma_\mu b\,, & O_4 &= O_{\partial S} = i\partial_\mu(\bar{s}b)\,. \end{aligned} \quad \text{(A.16)}$$

The mixing matrix is defined by

$$O_i^{(0)} = Z_q Z_{ij} O_j\,, \quad \text{(A.17)}$$

$B \to K^*$	$\mu^2[\,\mathrm{GeV}^2]$	$T_1(0)$	$V(0)$	$T_1(0)/V(0)$
pole	4.8	0.303	0.359	0.846
$\overline{\mathrm{MS}}$	4.8	0.290	0.347	0.837
$\overline{\mathrm{MS}}$	8	0.310	0.373	0.830

Table 10: As mentioned in the text the tensor form factors are understood to be evaluated at the scale $\mu_{\mathrm{UV}} = m_b$ by one-loop renormalisation group running. Note $\mu^2 = m_B^2 - m_b^2 \simeq 4.8\,\mathrm{GeV}^2$ is the standard factorisation scale of the LC-OPE used throughout. The values are for central values of the input parameters and differ slightly from that obtained from the Markov Chain Monte Carlo.

where Z_q is the external leg or wavefunction renormalisation. In $d = 4 - \epsilon$ we find

$$Z_{ij} = \delta_{ij} + C_F \frac{\alpha_s}{4\pi} \frac{1}{\epsilon} \begin{pmatrix} 2 & 2 & 6 & 6 \\ 0 & 0 & 0 & 0 \\ 0 & 0 & (2-6) & 0 \\ 0 & 0 & 0 & 8 \end{pmatrix} . \tag{A.18}$$

It is noteworthy that the renormalisation of the operator O_D requires the additional diagrams where a gluon originates from the vertex though the covariant derivative. The operators $O_{mV,\partial T,\partial S}$ do renormalise multiplicatively since they are of lowest dimension (effectively three) and differ in quantum numbers when the contraction of the total derivative is undone. The operator O_D is of dimension four and can and does mix with all the others. In the notation (A.16), the operator identity (5) reads

$$O_D + O_{mV} + O_{\partial T} - O_{\partial S} = 0 \,. \tag{A.19}$$

It is readily verified that the renormalisation (A.18) is compatible with (A.19). As an additional check let us mention that from the diagonal elements $Z_q \cdot \mathrm{diag}(Z) \equiv (Z_D, Z_{\partial T}, Z_m Z_V, Z_{\partial S})$ one infers $Z_S \equiv Z_{\partial_S} = 1 + 6\Delta$, $Z_V = 1$ and $Z_T \equiv Z_{\partial T} = 1 - 2\Delta$ with $\Delta = C_F \frac{\alpha_s}{4\pi} \frac{1}{\epsilon}$, $Z_m = 1 - 6\Delta$. From the latter the well-known anomalous dimensions $\gamma_S^{(0)} = -6C_F$, $\gamma_V^{(0)} = 0$ and $\gamma_T^{(0)} = 2C_F$ of these operators follow (notation: $\gamma_X = \gamma_X^{(0)} \frac{\alpha_s}{4\pi} + O(\alpha^2)$).

At last we turn to the issue of the impact of the mass renormalisation on the composite operators. From the mixing of operators in (A.18) it is clear that the renormalisation of O_D is affected by a mass scheme change. This can be seen by writing somewhat symbolically $Z_{13} = Z_{D(mV)} = Z_m Z_{DV}$. So in summary going to the pole scheme enforces a finite renormalisation of the operator O_D since changing from $\overline{\mathrm{MS}}$ to the pole scheme corresponds to a finite shift in the ratio of the Z_m-factors. Most importantly the renormalisation of the composite operators O_V, O_T and O_S, on the other hand, is not affected by the mass scheme. Hence it is legitimate to use the $\overline{\mathrm{MS}}$-scheme to renormalise them. This is fortunate since the Wilson coefficients are evaluated in the $\overline{\mathrm{MS}}$-scheme and together this guarantees the cancellation of the μ_{UV}-scale between the Wilson coefficients and the matrix elements. The scheme independence of the operators O_V, O_T underlies or partly explains the small changes in the form factors when going from the pole- to the $\overline{\mathrm{MS}}$-scheme (c.f. table 10).

A.6. Remarks on fixing the Borel parameter

A sum rule for a form factor $F(q^2)$ of a process $B \to P, V$-transition may be written as[19]

$$F(q^2)_{M^2} = \int_{m_b^2}^{s_0} \rho_F(s, q^2) e^{\frac{m_B^2 - s}{M^2}} ds \,, \tag{A.20}$$

where M^2 is the Borel parameter. The goal of this section is to show that two seemingly different methods for fixing M^2 are equivalent. For this purpose we introduce the following notation

$$\langle x(s) \rangle_{q^2, M^2} \equiv \int_{m_b^2}^{s_0} x(s) \rho_F(s, q^2) e^{\frac{m_B^2 - s}{M^2}} ds \,. \tag{A.21}$$

We note that $F(q^2)_{M^2} = \langle 1 \rangle_{q^2, M^2}$. The two methods are:

- *extremising the Borel parameter:* If one were to succeed in computing the sum rule exactly, which would imply[20]

  $$\rho_F(s, q^2) = \delta(s - m_B^2) F(q^2) + \Theta(s - s_c) \sigma_F(s) \,, \tag{A.22}$$

  then eq. (A.20) would remain valid for any Borel parameter. In practice the partonic evaluation through the OPE is optimised by using a large Borel parameter, just the opposite being true for the projection on the lowest hadronic state. Hence a compromise value has to be found, ideally in a region where $F(q^2)_{M^2}$ has an extremum in M^2. This is imposed by

  $$0 = \frac{d}{d(1/M^2)} \ln F(q^2)_{M^2} = \frac{m_B^2 \langle 1 \rangle_{q^2, M^2} - \langle s \rangle_{q^2, M^2}}{\langle 1 \rangle_{q^2, M^2}} \,. \tag{A.23}$$

- *daughter sum rule in m_B^2:* One may write a daughter sum rule for m_B^2 as follows

  $$(m_B^2)_{M^2} = \frac{\langle s \rangle_{q^2, M^2}}{\langle 1 \rangle_{q^2, M^2}} \,. \tag{A.24}$$

  Note that using eq. (A.22) satisfies (A.24) exactly as it should.

It is readily seen that eqs. (A.23,A.24) are the same and hence the two methods are equivalent.

B. Conversion between form factor bases

B.1. Helicity basis

In this appendix we give the projection of the form factors onto the helicity basis which is convenient for the computation of angular observables. Using the Jacob Wick polarisation tensors[21] we define:

$$X^{(\rho)} = \epsilon_\mu(\rho) \langle K^*(p, \eta(m(\rho))) | \bar{s} \Gamma_X^\mu b | \bar{B}(p_B) \rangle \,, \quad m(t) = m(0) = 0 \,, \; m(\pm) = \pm \tag{B.1}$$

[19] The relation between the density in eq. (A.20) and that in eq. (A.12) is $\rho_F(s, q^2) = \frac{m_b}{m_B^2 f_B} \bar{\rho}_F(u(s), q^2) \frac{(m_b^2 - q^2)}{(s - q^2)^2}$ through the change of variable $u(s) = (m_b^2 - q^2)/(s - q^2)$.

[20] For the sake of illustration we employ the narrow width approximation which should be justified for the B-meson.

[21] C.f. appendix A [60] where the polarisation tensors η and ϵ correspond to γ and β respectively.

where $\rho = 0, \pm, t$ is the polarisation index which is not summed over and $\Gamma_T^\mu = iq_\nu\sigma^{\mu\nu}(1 \pm \gamma_5)$, $\Gamma_{\mathcal{V}}^\mu = \gamma^\mu(1 \mp \gamma_5)$ and $\Gamma_{\mathcal{D}}^\mu = (2i \overleftarrow{D})^\mu(1 \pm \gamma_5)$ correspond to tensor, vector and derivative form factors. We get

$$\begin{aligned}
X^{(\perp)} &= \frac{1}{\sqrt{2}}(X^{(+)} - X^{(-)}) = i\sqrt{2}\sqrt{\lambda(q^2)}X_1 \,, \\
X^{(\parallel)} &= \frac{1}{\sqrt{2}}(X^{(+)} + X^{(-)}) = \pm i\sqrt{2}(m_B^2 - m_{K^*}^2)X_2 \,, \\
X^{(0)} &= \mp i\frac{\sqrt{q^2}(m_B^2 + 3m_V^2 - q^2)}{2m_{K^*}}X_0 \,, \\
X^{(t)} &= \mp i\frac{\sqrt{\lambda(q^2)}}{2}X_P
\end{aligned} \tag{B.2}$$

where $X_0 \equiv X_2 - c_{23}(q^2)X_3$ with

$$\begin{aligned}
c_{23}(q^2) &\equiv \frac{\lambda(q^2)}{(m_B^2 - m_{K^*}^2)(m_B^2 + 3m_{K^*}^2 - q^2)} \,, \\
\lambda(q^2) &\equiv ((m_B + m_{K^*})^2 - q^2)((m_B - m_{K^*})^2 - q^2) \,,
\end{aligned} \tag{B.3}$$

and λ being the Källén-function. We infer that at the kinematic endpoint where $\lambda = 0$ only the X_2 structure contributes in accordance with general findings on endpoint symmetries [60].

For $X = T, \mathcal{V}, \mathcal{D}$, X_i is given by T_i (with $T_P \equiv 0$) $\mathcal{V}_i$ and $\mathcal{D}_\iota$ in eq. (3) and (10) respectively. The relation of T_0 and $\mathcal{V}_0$ to T_{23} and A_{12} used in the literature (e.g. [39]) is as follows:

$$T_0 = \frac{8m_B m_{K^*}^2}{(m_B + m_{K^*})(m_B^2 + 3m_{K^*}^2 - q^2)}T_{23} \,, \quad \mathcal{V}_0 = \frac{-16m_B m_{K^*}^2}{q^2(m_B^2 + 3m_{K^*}^2 - q^2)}A_{12} \tag{B.4}$$

where

$$\begin{aligned}
A_{12} &= \frac{(m_B + m_{K^*})^2\left(m_B^2 - m_{K^*}^2 - q^2\right)A_1 - \lambda(q^2)A_2}{16m_B m_{K^*}^2\,(m_B + m_{K^*})} \\
&= \frac{q^2/2(m_B^2 + 3m_{K^*}^2 - q^2)A_1 + \lambda(q^2)m_{K^*}/(m_B + m_{K^*})A_3}{8m_B m_{K^*}^2(m_B - m_{K^*})} \\
T_{23} &= \frac{\left(m_B^2 - m_{K^*}^2\right)\left(m_B^2 + 3m_{K^*}^2 - q^2\right)T_2 - \lambda(q^2)T_3}{8m_B m_{K^*}^2\,(m_B - m_{K^*})}.
\end{aligned} \tag{B.5}$$

We further notice that

$$A_{12}(0) = \frac{m_B^2 - m_{K^*}^2}{8m_B m_{K^*}}A_3(0) = \frac{m_B^2 - m_{K^*}^2}{8m_B m_{K^*}}A_0(0) \,, \tag{B.6}$$

which we implement, besides $T_1(0) = T_2(0)$, into the fit as a constraint.

C. Plots of form factors as a function of z

The plots of the form factors in the z-variable can be found in figs. 5,6, and 7 for the modes $B \to K^*$, $B_s \to \phi$ and $B_s \to \bar{K}^*$, respectively.

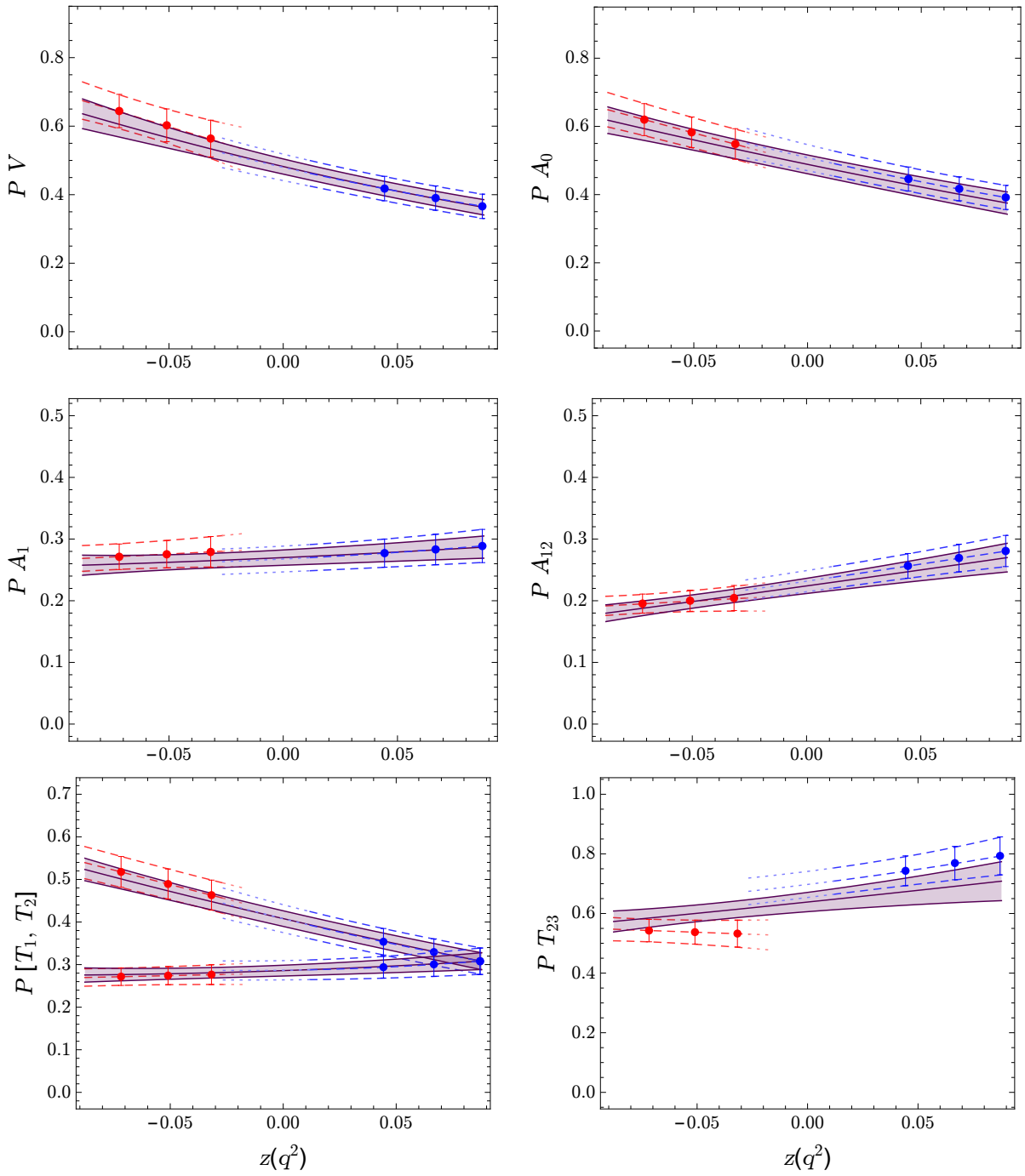

Figure 5: Combined LCSR and lattice fit to $B \to K^*$ form factors, where lattice data points are indicated in red, LCSR points in blue, the gray solid band shows the combined 3-parameter fit and the red dashed band the 2-parameter lattice fit from ref. [39].

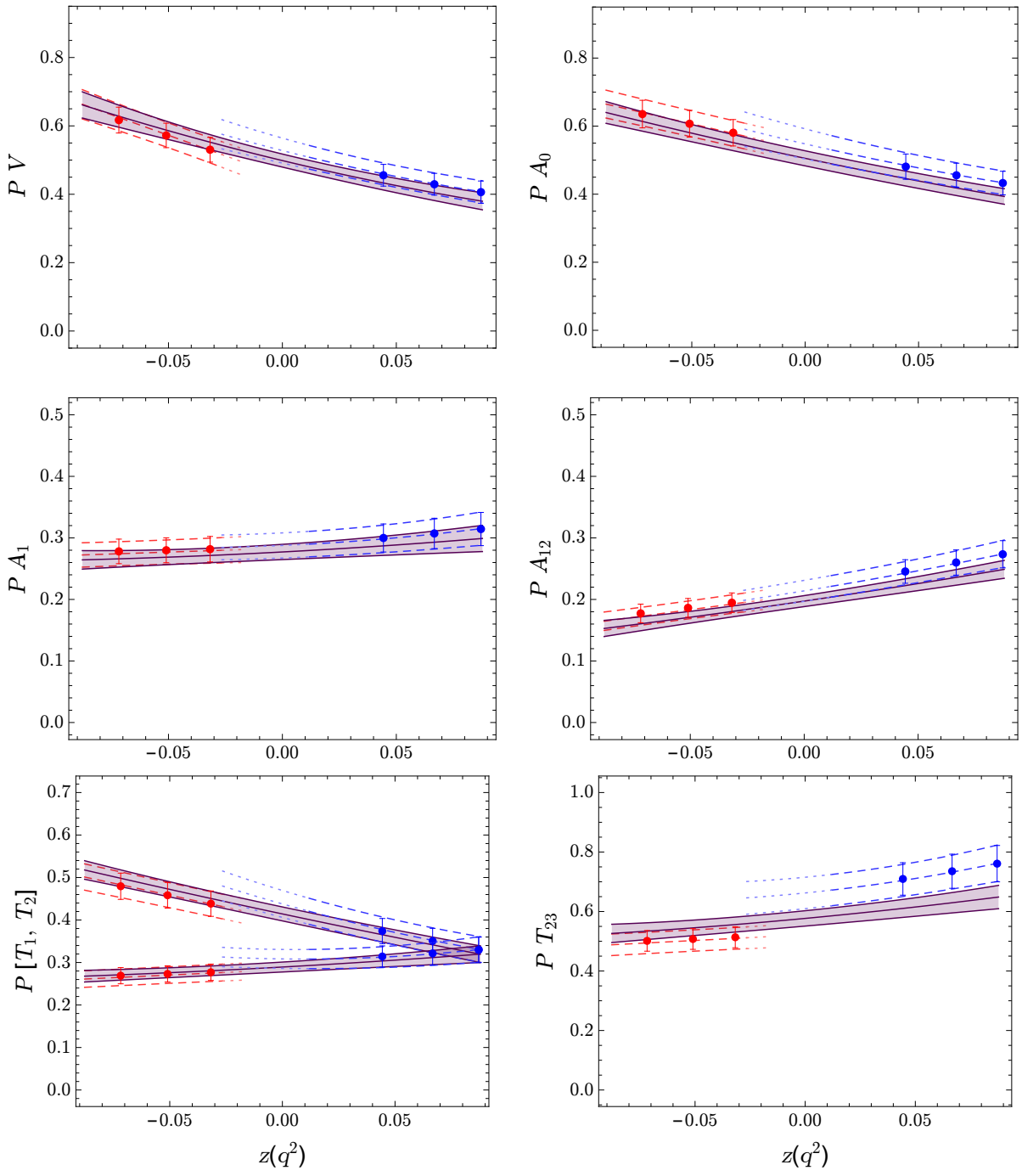

Figure 6: Combined LCSR and lattice fit to $B_s \to \phi$ form factors, where lattice data points are indicated in red, LCSR points in blue, the gray solid band shows the combined 3-parameter fit and the red dashed band the 2-parameter lattice fit from ref. [39].

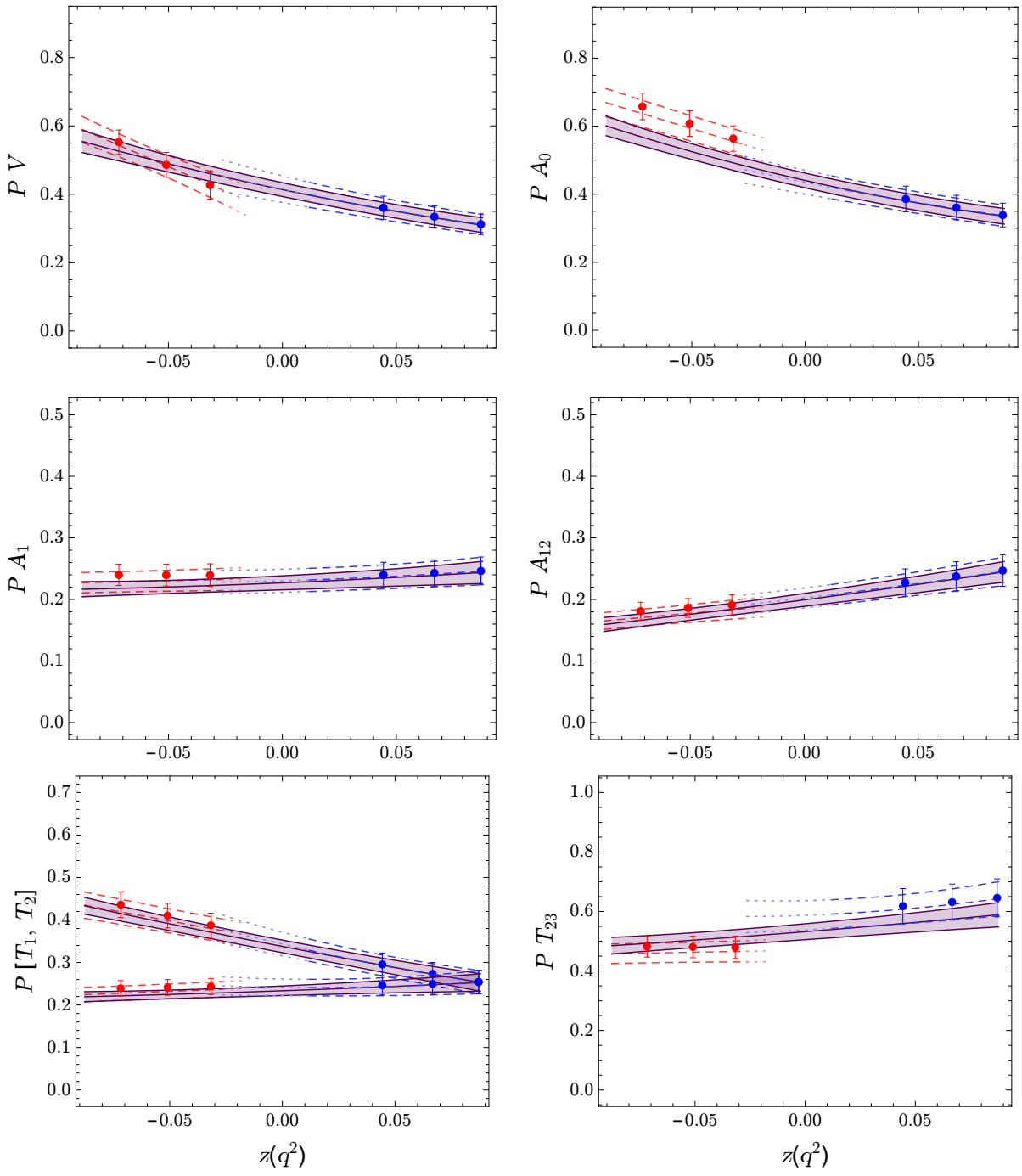

Figure 7: Combined LCSR and lattice fit to $B_s \to \bar{K}^*$ form factors, where lattice data points are indicated in red, LCSR points in blue, the gray solid band shows the combined 3-parameter fit and the red dashed band the 2-parameter lattice fit from ref. [39].

D. SSE coefficients

In this appendix we list the central values and uncertainties of the SSE expansion coefficients of the $B \to K^*$, $B \to \rho$, $B \to \omega$, $B_s \to \phi$ and $B_s \to \bar{K}^*$ form factors from LCSR (table 11) as well as the combined fits to LCSR and lattice data for the $B \to K^*$ and $B_s \to \phi$ form factors (table 12). Note that of the 21 parameters for each transition, two are in fact redundant due to the exact relations (16).

In addition to these central values and uncertainties, we also provide the full correlation and covariance matrices as ancillary files downloadable from the arXiv preprint page. The data are contained in 5 JSON files named `[Process]_[Fit].json`, where `[Process]` is `BKstar` for $B \to K^*$, `Brho` for $B \to \rho$, `Bomega` for $B \to \omega$, `Bsphi` for $B_s \to \phi$ and `BsKstar` for $B_s \to \bar{K}^*$ form factors; `[Fit]` is `LCSR` for the fit to LCSR only (valid at low q^2) and `LCSR-Lattice` for the combined fit valid in the full q^2 range.

The JSON format can be easily used in `Mathematica`. For example, reading in the file for the $B \to K^*$ LCSR form factors,

```
data = Import["BKstar_LCSR.json"]
```

the central value of $\alpha_0^{T_1}$ can be accessed simply via

```
OptionValue[data, "central" -> "T1" -> "a0"]
```

and the correlation between $\alpha_1^{A_0}$ and α_2^V as

```
OptionValue[data, "correlation" -> "A0V" -> "a1a2"]
```

and similarly for the objects `"uncertainty"` and `"covariance"`. In Python, the corresponding commands would read

```
import json
with open('BKstar_LCSR.json') as file:
  data = json.load(file)
```

and the parameters can be accessed via

```
data['central']['T1']['a0']
data['correlation']['A0V']['a1a2']
```

etc.

E. Lifetime effect in $B_s \to \phi\mu^+\mu^-$

To compare the experimental measurement of the $B_s \to \phi\mu\mu$ branching ratio and angular observables from an untagged data sample to the theoretical predictions, the difference in finite width $\Delta\Gamma_s$ between the B_s mass eigenstates of widths Γ_L and Γ_H has to be taken into account. This leads to a difference between experimentally accessible time-integrated CP-averaged observables $\mathcal{O}_{\text{exp}}$ and the theoretical definition of CP-averaged observables $\mathcal{O}_{\text{theo}}$ in the flavour eigenstate basis. The former and the latter are defined as

$$\mathcal{O}_{\text{exp}} = \int_0^\infty \frac{dt}{\tau_{B_s}} \mathcal{O}(t)\,, \qquad\qquad \mathcal{O}_{\text{theo}} = \mathcal{O}(t=0)\,, \tag{E.1}$$

	$B \to K^*$	$B \to \rho$	$B \to \omega$	$B_s \to \phi$	$B_s \to K^*$
$\alpha_0^{A_0}$	0.39 ± 0.04	0.37 ± 0.03	0.31 ± 0.04	0.43 ± 0.04	0.34 ± 0.03
$\alpha_1^{A_0}$	-1.15 ± 0.28	-0.99 ± 0.23	-0.90 ± 0.30	-1.06 ± 0.30	-0.93 ± 0.24
$\alpha_2^{A_0}$	2.08 ± 1.50	1.17 ± 1.21	1.19 ± 1.18	2.74 ± 1.52	2.22 ± 1.43
$\alpha_0^{A_1}$	0.29 ± 0.03	0.27 ± 0.02	0.24 ± 0.03	0.32 ± 0.03	0.25 ± 0.02
$\alpha_1^{A_1}$	0.31 ± 0.19	0.36 ± 0.13	0.34 ± 0.19	0.46 ± 0.22	0.26 ± 0.19
$\alpha_2^{A_1}$	0.72 ± 0.49	0.55 ± 0.35	0.55 ± 0.46	1.70 ± 0.83	0.86 ± 0.70
$\alpha_0^{A_{12}}$	0.28 ± 0.03	0.31 ± 0.03	0.26 ± 0.03	0.27 ± 0.02	0.25 ± 0.02
$\alpha_1^{A_{12}}$	0.57 ± 0.22	0.67 ± 0.20	0.51 ± 0.25	0.77 ± 0.18	0.55 ± 0.18
$\alpha_2^{A_{12}}$	0.14 ± 0.86	0.33 ± 0.75	0.15 ± 0.90	0.91 ± 1.00	0.68 ± 0.95
α_0^{V}	0.37 ± 0.04	0.33 ± 0.03	0.30 ± 0.04	0.41 ± 0.03	0.31 ± 0.03
α_1^{V}	-1.08 ± 0.24	-0.89 ± 0.18	-0.77 ± 0.24	-1.06 ± 0.30	-0.93 ± 0.33
α_2^{V}	2.47 ± 1.35	1.74 ± 1.13	1.49 ± 0.94	3.66 ± 1.54	2.89 ± 1.84
$\alpha_0^{T_1}$	0.31 ± 0.03	0.28 ± 0.03	0.25 ± 0.03	0.33 ± 0.03	0.25 ± 0.03
$\alpha_1^{T_1}$	-0.96 ± 0.20	-0.78 ± 0.14	-0.67 ± 0.19	-0.94 ± 0.23	-0.80 ± 0.30
$\alpha_2^{T_1}$	2.01 ± 1.09	1.51 ± 0.93	1.29 ± 0.74	3.20 ± 1.30	2.55 ± 1.42
$\alpha_0^{T_2}$	0.31 ± 0.03	0.28 ± 0.03	0.25 ± 0.03	0.33 ± 0.03	0.25 ± 0.03
$\alpha_1^{T_2}$	0.42 ± 0.20	0.47 ± 0.14	0.45 ± 0.19	0.58 ± 0.21	0.36 ± 0.24
$\alpha_2^{T_2}$	2.02 ± 0.72	1.58 ± 0.60	1.48 ± 0.57	3.69 ± 1.13	2.44 ± 1.05
$\alpha_0^{T_{23}}$	0.79 ± 0.06	0.81 ± 0.08	0.70 ± 0.08	0.76 ± 0.06	0.64 ± 0.06
$\alpha_1^{T_{23}}$	1.26 ± 0.61	1.45 ± 0.51	1.19 ± 0.63	1.55 ± 0.47	0.99 ± 0.49
$\alpha_2^{T_{23}}$	1.96 ± 2.38	2.50 ± 1.72	1.97 ± 2.11	4.59 ± 2.51	4.03 ± 2.45

Table 11: Fit results for the SSE expansion coefficients in the fit to the LCSR computation only. These numbers are provided (to higher accuracy) in electronic form along with the full correlation matrices as arXiv ancillary files.

where τ_{B_s} is the lifetime of the B_s

$$\mathcal{O}(t)(B_s \to \phi\mu^+\mu^-) = \frac{1}{2}\left[\mathcal{O}(B_s(t) \to \phi\mu^+\mu^-) + \mathcal{O}(\bar{B}_s(t) \to \phi\mu^+\mu^-)\right] . \tag{E.2}$$

In the case where only vector operators are present (i.e. $H_{\text{eff}} \sim \bar{b}\gamma_\mu(\gamma_5)s\bar{\ell}\gamma^\mu(\gamma_5)\ell$), the time-dependent CP-averaged observables $\mathcal{O}(t)$ can be written as functions $F_\mathcal{O}$ of bilinears of time-dependent transversity amplitudes $\mathcal{J}_{bX,aY}(t)$

$$\mathcal{O}(t) = F_\mathcal{O}(\mathcal{J}_{bX,aY}(t)) , \tag{E.3}$$

$$\mathcal{J}_{bX,aY}(t) = A_b^X(t)A_a^Y(t)^* + \bar{A}_b^X(t)\bar{A}_a^Y(t)^* , \tag{E.4}$$

where $a, b = 0, \|, \perp$ are the vector meson polarisation indices and $X, Y = L, R$ denote the chirality structure of the lepton production. The CP-conjugated amplitude is

$$\bar{A}_a^{L,R} = \eta_a A_a^{R,L}(\phi_w \to -\phi_w) , \tag{E.5}$$

	$B \to K^*$	$B_s \to \phi$	$B_s \to K^*$
$a_0^{A_0}$	0.38 ± 0.03	0.39 ± 0.02	0.33 ± 0.02
$a_1^{A_0}$	-1.20 ± 0.31	-1.15 ± 0.21	-0.89 ± 0.19
$a_2^{A_0}$	1.03 ± 1.54	1.46 ± 1.21	3.58 ± 1.31
$a_0^{A_1}$	0.29 ± 0.02	0.30 ± 0.02	0.24 ± 0.02
$a_1^{A_1}$	0.22 ± 0.18	0.30 ± 0.19	0.23 ± 0.17
$a_2^{A_1}$	0.31 ± 1.01	0.59 ± 0.83	0.42 ± 0.75
$a_0^{A_{12}}$	0.27 ± 0.02	0.25 ± 0.01	0.24 ± 0.02
$a_1^{A_{12}}$	0.53 ± 0.18	0.63 ± 0.10	0.55 ± 0.12
$a_2^{A_{12}}$	0.11 ± 0.79	0.47 ± 0.60	0.37 ± 0.59
a_0^{V}	0.36 ± 0.02	0.38 ± 0.02	0.31 ± 0.02
a_1^{V}	-1.16 ± 0.25	-1.11 ± 0.27	-0.97 ± 0.29
a_2^{V}	2.26 ± 1.71	2.84 ± 1.55	2.40 ± 1.49
$a_0^{T_1}$	0.31 ± 0.02	0.32 ± 0.02	0.25 ± 0.02
$a_1^{T_1}$	-1.05 ± 0.22	-1.03 ± 0.21	-0.90 ± 0.27
$a_2^{T_1}$	0.99 ± 1.14	0.56 ± 0.89	0.70 ± 0.98
$a_0^{T_2}$	0.31 ± 0.02	0.32 ± 0.02	0.25 ± 0.02
$a_1^{T_2}$	0.32 ± 0.18	0.40 ± 0.17	0.25 ± 0.19
$a_2^{T_2}$	0.77 ± 0.88	0.58 ± 0.76	0.34 ± 0.80
$a_0^{T_{23}}$	0.71 ± 0.07	0.65 ± 0.04	0.59 ± 0.04
$a_1^{T_{23}}$	0.82 ± 0.59	0.94 ± 0.31	0.71 ± 0.37
$a_2^{T_{23}}$	0.31 ± 2.32	1.38 ± 1.52	0.65 ± 1.69

Table 12: Fit results for the SSE expansion coefficients in the combined LCSR + lattice fit. These numbers are provided (to higher accuracy) in electronic form along with the full correlation matrices as arXiv ancillary files.

where $\eta_{\parallel,0} = +1$ and $\eta_\perp = -1$ are the CP-eigenvalues of the amplitudes and $(\phi_w \to -\phi_w)$ refers to the conjugation of all weak (CP-odd) phases. Defining the quantity (as in e.g. ref. [74])

$$\xi_a^\lambda = -e^{-i\phi_s} \frac{A_a^\lambda}{\bar{A}_a^\lambda} \,, \tag{E.6}$$

where ϕ_s the B_s mixing phase, one can write

$$\mathcal{J}_{bX,aY}(t) = \mathcal{J}_{bX,aY}(0) \frac{1}{2} \left[(e^{-\Gamma_L t} + e^{-\Gamma_H t}) - \mathcal{A}_{\Delta\Gamma}^{bX,aY} (e^{-\Gamma_L t} - e^{-\Gamma_H t}) \right] \,, \tag{E.7}$$

with

$$\mathcal{A}_{\Delta\Gamma}^{bX,aY} \equiv -\frac{\xi_b^{X*} + \xi_a^Y}{1 + \xi_b^{X*} \xi_a^Y} \,. \tag{E.8}$$

In summary for the experimental and theoretical expression in (E.1), we obtain

$$\begin{aligned} J_{bX,aY}|_{\rm exp} &= \int_0^\infty \frac{dt}{\tau_{B_s}}\,\mathcal{J}_{bX,aY}(t) = \frac{1+y_s\mathcal{A}_{\Delta\Gamma}^{bX,aY}}{1-y_s^2}\mathcal{J}_{bX,aY}(0)\,, \\ J_{bX,aY}|_{\rm theo} &= \mathcal{J}_{bX,aY}(0)\,, \end{aligned} \tag{E.9}$$

where

$$y_s \equiv \frac{\Gamma_L-\Gamma_H}{\Gamma_L+\Gamma_H}\,, \quad \frac{1}{\tau_{B_s}} = \frac{1}{2}(\Gamma_L+\Gamma_H)\,. \tag{E.10}$$

As a simple example, we consider the differential branching ratio at low q^2 in the SM, within naive factorisation and in the heavy quark and massless lepton limit, where the transversity amplitudes read

$$\begin{aligned} A_\perp^{L,R} &= \sqrt{2}Nm_{B_s}(1-\hat{s})\left(C_9^{\rm eff}\mp C_{10}+\frac{2m_bm_B}{q^2}C_7^{\rm eff}\right)\xi_\perp\,, \\ A_\parallel^{L,R} &= -A_\perp^{L,R}\,, \\ A_0^{L,R} &= -\frac{Nm_{B_s}^2(1-\hat{s})^2}{2m_\phi\sqrt{\hat{s}}}\left(C_9^{\rm eff}\mp C_{10}+\frac{2m_b}{m_B}C_7^{\rm eff}\right)\xi_\parallel\,, \end{aligned} \tag{E.11}$$

with $\hat{s}=q^2/m_{B_s}^2$ and N being a normalisation factor including the CKM elements $V_{tb}V_{ts}^*$. Note the soft form factors $\xi_{\parallel,\perp}$ are not to be confused with the ratio of amplitudes in (E.6). One finds

$$\begin{aligned} \xi_\perp^L &= \frac{C_9^{\rm eff}-C_{10}+\frac{2m_bm_B}{q^2}C_7^{\rm eff}}{C_9^{\rm eff}+C_{10}+\frac{2m_bm_B}{q^2}C_7^{\rm eff}}\,, \\ \xi_\parallel^L &= -\xi_\perp^L\,, \\ \xi_0^L &= -\frac{C_9^{\rm eff}-C_{10}+\frac{2m_b}{m_B}C_7^{\rm eff}}{C_9^{\rm eff}+C_{10}+\frac{2m_b}{m_B}C_7^{\rm eff}}\,, \\ \xi_{\parallel,\perp,0}^R &= 1/(\xi_{\parallel,\perp,0}^L)\,. \end{aligned} \tag{E.12}$$

The theoretical and experimental CP-averaged differential branching ratio in the assumed limit read

$$\begin{aligned} \left.\frac{d\overline{\rm BR}}{dq^2}\right|_{\rm theo} &= \tau_{B_s}\left(|A_\perp^L|^2+|A_\perp^R|^2+|A_\parallel^L|^2+|A_\parallel^R|^2+|A_0^L|^2+|A_0^R|^2\right) \\ &= \tau_{B_s}\left[2\left(|A_\perp^L|^2+|A_\perp^R|^2\right)+|A_0^L|^2+|A_0^R|^2\right] \end{aligned} \tag{E.13}$$

and

$$\begin{aligned} \left.\frac{d\overline{\rm BR}}{dq^2}\right|_{\rm exp} &= \tau_{B_s}\sum_{a=\perp,\parallel,0}\left(\frac{1+y_s\mathcal{A}_{\Delta\Gamma}^a}{1-y_s^2}\right)\left(|A_a^L|^2+|A_a^R|^2\right) \\ &= \tau_{B_s}\left[\frac{2}{1-y_s^2}\left(|A_\perp^L|^2+|A_\perp^R|^2\right)+\left(\frac{1+y_s\mathcal{A}_{\Delta\Gamma}^0}{1-y_s^2}\right)\left(|A_0^L|^2+|A_0^R|^2\right)\right]\,, \end{aligned} \tag{E.14}$$

where

$$\mathcal{A}_{\Delta\Gamma}^a = \mathcal{A}_{\Delta\Gamma}^{aL,aL} = \mathcal{A}_{\Delta\Gamma}^{aR,aR} = -\frac{2}{(\xi_a^L)^{-1}+\xi_a^L}\,,$$

which implies $\mathcal{A}^{\parallel}_{\Delta\Gamma} = -\mathcal{A}^{\perp}_{\Delta\Gamma}$. Expanding this expression in y_s, the only linear term is proportional to $\mathcal{A}^{0}_{\Delta\Gamma}$. As a result of $A_0^L = 1/A_0^R \ll 1$ in the SM it turns out that $\mathcal{A}^{0}_{\Delta\Gamma}$ is only of order 0.1. This is a numerical coincidence due to $C_9^{\text{eff}} \approx -C_{10}$ as well as $C_7^{\text{eff}} \ll C_9^{\text{eff}}$. Consequently, since $y_s \simeq \mathcal{O}(0.1)$ the overall effect is of order y_s^2 and thus small in view of the theoretical uncertainties. This is in agreement with the findings of ref. [75].

Restoring the full expressions without making any approximation, we have checked numerically that the corrections to the branching ratio and all angular observables are at the 1% level and thus negligible in the SM. This conclusion changes however when new physics contributions are allowed, in particular in the presence of the right-handed Wilson coefficients $C'_{7,9,10}$. In that case, differences of several percent arise. as investigated in ref. [75].

References

[1] P. Ball and R. Zwicky, *$B_{d,s} \to \rho, \omega, K^*, \phi$ decay form-factors from light-cone sum rules revisited*, *Phys.Rev.* **D71** (2005) 014029, [hep-ph/0412079].

[2] C. Hambrock, G. Hiller, S. Schacht, and R. Zwicky, *$B \to K^*$ Form Factors from Flavor Data to QCD and Back*, arXiv:1308.4379.

[3] J. Charles, A. Le Yaouanc, L. Oliver, O. Pene, and J. Raynal, *Heavy to light form-factors in the heavy mass to large energy limit of QCD*, *Phys.Rev.* **D60** (1999) 014001, [hep-ph/9812358].

[4] M. Beneke and T. Feldmann, *Symmetry breaking corrections to heavy to light B meson form-factors at large recoil*, *Nucl.Phys.* **B592** (2001) 3–34, [hep-ph/0008255].

[5] S. Descotes-Genon, L. Hofer, J. Matias, and J. Virto, *On the impact of power corrections in the prediction of $B \to K^*\mu^+\mu^-$ observables*, arXiv:1407.8526.

[6] S. Descotes-Genon, T. Hurth, J. Matias, and J. Virto, *Optimizing the basis of $B \to K^*\ell^+\ell^-$ observables in the full kinematic range*, *JHEP* **1305** (2013) 137, [arXiv:1303.5794].

[7] J. Lyon and R. Zwicky, *Isospin asymmetries in $B \to (K^*, \rho)/l^+l^-$ and $B \to Kl^+l^-$ in and beyond the standard model*, *Phys.Rev.* **D88** (2013), no. 9 094004, [arXiv:1305.4797].

[8] M. A. Shifman, A. Vainshtein, and V. I. Zakharov, *QCD and Resonance Physics. Sum Rules*, *Nucl.Phys.* **B147** (1979) 385–447.

[9] M. A. Shifman, A. Vainshtein, and V. I. Zakharov, *QCD and Resonance Physics. The ρ-ω Mixing*, *Nucl.Phys.* **B147** (1979) 519.

[10] I. Balitsky, V. M. Braun, and A. Kolesnichenko, *Radiative Decay $\Sigma^+ \to p\gamma$ in Quantum Chromodynamics*, *Nucl.Phys.* **B312** (1989) 509–550.

[11] V. Chernyak and I. Zhitnitsky, *B meson exclusive decays into baryons*, *Nucl.Phys.* **B345** (1990) 137–172.

[12] P. Ball and V. M. Braun, *Exclusive semileptonic and rare B meson decays in QCD*, *Phys.Rev.* **D58** (1998) 094016, [hep-ph/9805422].

[13] A. Khodjamirian, T. Mannel, and N. Offen, *Form-factors from light-cone sum rules with B-meson distribution amplitudes*, *Phys.Rev.* **D75** (2007) 054013, [hep-ph/0611193].

[14] B. Grinstein and D. Pirjol, *Exclusive rare $B \to K^* \ell^+ \ell^-$ decays at low recoil: Controlling the long-distance effects*, *Phys.Rev.* **D70** (2004) 114005, [hep-ph/0404250].

[15] N. Isgur and M. B. Wise, *Relationship Between Form-factors in Semileptonic $\bar{B}$ and D Decays and Exclusive Rare $\bar{B}$ Meson Decays*, *Phys.Rev.* **D42** (1990) 2388–2391.

[16] M. Diehl, T. Gousset, B. Pire, and O. Teryaev, *Probing partonic structure in $\gamma^* \gamma \to \pi\pi$ near threshold*, *Phys.Rev.Lett.* **81** (1998) 1782–1785, [hep-ph/9805380].

[17] M. V. Polyakov, *Hard exclusive electroproduction of two pions and their resonances*, *Nucl.Phys.* **B555** (1999) 231, [hep-ph/9809483].

[18] N. Kivel, L. Mankiewicz, and M. V. Polyakov, *NLO corrections and contribution of a tensor gluon operator to the process $\gamma^* \gamma \to \pi\pi$*, *Phys.Lett.* **B467** (1999) 263–270, [hep-ph/9908334].

[19] M. Diehl, *Generalized parton distributions*, *Phys.Rept.* **388** (2003) 41–277, [hep-ph/0307382].

[20] R. A. Briceo, M. T. Hansen, and A. Walker-Loud, *Multichannel $1 \to 2$ transition amplitudes in a finite volume*, *Phys.Rev.* **D91** (2015), no. 3 034501, [arXiv:1406.5965].

[21] D. Becirevic and A. Tayduganov, *Impact of $B \to K_0^* \ell^+ \ell^-$ on the New Physics search in $B \to K^* \ell^+ \ell^-$ decay*, *Nucl.Phys.* **B868** (2013) 368–382, [arXiv:1207.4004].

[22] U.-G. Meiner and W. Wang, *Generalized Heavy-to-Light Form Factors in Light-Cone Sum Rules*, *Phys.Lett.* **B730** (2014) 336–341, [arXiv:1312.3087].

[23] **CLEO Collaboration** Collaboration, B. Behrens et al., *Measurement of $B \to \rho \ell \nu$ decay and $|V_{ub}|$*, *Phys.Rev.* **D61** (2000) 052001, [hep-ex/9905056].

[24] **CLEO Collaboration** Collaboration, N. Adam et al., *A Study of Exclusive Charmless Semileptonic B Decay and $|V_{ub}|$*, *Phys.Rev.Lett.* **99** (2007) 041802, [hep-ex/0703041].

[25] P. Ball, G. W. Jones, and R. Zwicky, *$B \to V\gamma$ beyond QCD factorisation*, *Phys.Rev.* **D75** (2007) 054004, [hep-ph/0612081].

[26] W. are grateful to Gilberto Colangelo, P. S. for providing with the necessary plots, and their insights into this matter.

[27] U.-G. Meiner and W. Wang, *$\mathbf{B_s \to K^{(*)} \ell \bar{\nu}}$, Angular Analysis, S-wave Contributions and $\mathbf{|V_{ub}|}$*, *JHEP* **1401** (2014) 107, [arXiv:1311.5420].

[28] S. Faller, T. Feldmann, A. Khodjamirian, T. Mannel, and D. van Dyk, *Disentangling the Decay Observables in $B^- \to \pi^+ \pi^- \ell^- \bar{\nu}_\ell$*, *Phys.Rev.* **D89** (2014), no. 1 014015, [arXiv:1310.6660].

[29] X.-W. Kang, B. Kubis, C. Hanhart, and U.-G. Meiner, *B_{l4} decays and the extraction of $|V_{ub}|$*, *Phys.Rev.* **D89** (2014), no. 5 053015, [arXiv:1312.1193].

[30] G. Colangelo, E. Passemar, and P. Stoffer, *A Dispersive Treatment of $K_{\ell 4}$ Decays*, arXiv:1501.0562.

[31] P. Ball and G. Jones, *Twist-3 distribution amplitudes of K^* and ϕ mesons*, *JHEP* **0703** (2007) 069, [hep-ph/0702100].

[32] M. Dimou, J. Lyon, and R. Zwicky, *Heavy-to-light chromomagnetic matrix element*, *Nucl.Phys.Proc.Suppl.* **241-242** (2013) 127–132.

[33] **Particle Data Group** Collaboration, K. Olive et al., *Review of Particle Physics*, *Chin.Phys.* **C38** (2014) 090001.

[34] A. Bharucha, *Two-loop Corrections to the $B \to \pi$ Form Factor from QCD Sum Rules on the Light-Cone and $|V_{ub}|$*, *JHEP* **1205** (2012) 092, [arXiv:1203.1359].

[35] T. Aliev and V. Eletsky, *On Leptonic Decay Constants of Pseudoscalar D and B Mesons*, *Sov.J.Nucl.Phys.* **38** (1983) 936.

[36] E. Bagan, P. Ball, V. M. Braun, and H. G. Dosch, *QCD sum rules in the effective heavy quark theory*, *Phys.Lett.* **B278** (1992) 457–464.

[37] P. Ball and R. Zwicky, *New results on $B \to \pi, K, \eta$ decay formfactors from light-cone sum rules*, *Phys.Rev.* **D71** (2005) 014015, [hep-ph/0406232].

[38] A. Bharucha, T. Feldmann, and M. Wick, *Theoretical and Phenomenological Constraints on Form Factors for Radiative and Semi-Leptonic B-Meson Decays*, *JHEP* **1009** (2010) 090, [arXiv:1004.3249].

[39] R. R. Horgan, Z. Liu, S. Meinel, and M. Wingate, *Lattice QCD calculation of form factors describing the rare decays $B \to K^* \ell^+ \ell^-$ and $B_s \to \phi \ell^+ \ell^-$*, *Phys.Rev.* **D89** (2014) 094501, [arXiv:1310.3722].

[40] **LHCb** Collaboration, R. Aaij et al., *Differential branching fraction and angular analysis of the decay $B^0 \to K^{*0} \mu^+ \mu^-$*, *JHEP* **1308** (2013) 131, [arXiv:1304.6325].

[41] **LHCb** Collaboration, R. Aaij et al., *Measurement of Form-Factor-Independent Observables in the Decay $B^0 \to K^{*0} \mu^+ \mu^-$*, *Phys.Rev.Lett.* **111** (2013), no. 19 191801, [arXiv:1308.1707].

[42] **LHCb** Collaboration, R. Aaij et al., *Differential branching fractions and isospin asymmetries of $B \to K^{(*)} \mu^+ \mu^-$ decays*, *JHEP* **1406** (2014) 133, [arXiv:1403.8044].

[43] **CMS** Collaboration, S. Chatrchyan et al., *Angular analysis and branching fraction measurement of the decay $B^0 \to K^{*0} \mu^+ \mu^-$*, *Phys.Lett.* **B727** (2013) 77–100, [arXiv:1308.3409].

[44] **ATLAS** Collaboration, *Angular Analysis of $B_d \to K^{*0} \mu^+ \mu^-$ with the ATLAS Experiment*, .

[45] S. Descotes-Genon, J. Matias, and J. Virto, *Understanding the $B \to K^* \mu^+ \mu^-$ Anomaly*, *Phys.Rev.* **D88** (2013), no. 7 074002, [arXiv:1307.5683].

[46] W. Altmannshofer and D. M. Straub, *New physics in $B \to K^* \mu\mu$?*, *Eur.Phys.J.* **C73** (2013), no. 12 2646, [arXiv:1308.1501].

[47] F. Beaujean, C. Bobeth, and D. van Dyk, *Comprehensive Bayesian analysis of rare (semi)leptonic and radiative B decays*, *Eur.Phys.J.* **C74** (2014), no. 6 2897, [arXiv:1310.2478].

[48] J. Lyon and R. Zwicky, *Resonances gone topsy turvy - the charm of QCD or new physics in $b \to s\ell^+\ell^-$?*, arXiv:1406.0566.

[49] W. Altmannshofer and D. M. Straub, *State of new physics in $b \to s$ transitions*, arXiv:1411.3161.

[50] S. Jger and J. Martin Camalich, *Reassessing the discovery potential of the $B \to K^* \ell^+ \ell^-$ decays in the large-recoil region: SM challenges and BSM opportunities*, arXiv:1412.3183.

[51] W. Altmannshofer, P. Ball, A. Bharucha, A. J. Buras, D. M. Straub, et al., *Symmetries and Asymmetries of $B \to K^* \mu^+ \mu^-$ Decays in the Standard Model and Beyond*, *JHEP* **0901** (2009) 019, [arXiv:0811.1214].

[52] H. Asatryan, H. Asatrian, C. Greub, and M. Walker, *Calculation of two loop virtual corrections to b —¿ s l+ l- in the standard model*, *Phys.Rev.* **D65** (2002) 074004, [hep-ph/0109140].

[53] M. Dimou, J. Lyon, and R. Zwicky, *Exclusive Chromomagnetism in heavy-to-light FCNCs*, *Phys.Rev.* **D87** (2013), no. 7 074008, [arXiv:1212.2242].

[54] M. Beneke, T. Feldmann, and D. Seidel, *Systematic approach to exclusive $B \to V l^+ l^-, V\gamma$ decays*, *Nucl.Phys.* **B612** (2001) 25–58, [hep-ph/0106067].

[55] M. Beneke, T. Feldmann, and D. Seidel, *Exclusive radiative and electroweak $b \to d$ and $b \to s$ penguin decays at NLO*, *Eur.Phys.J.* **C41** (2005) 173–188, [hep-ph/0412400].

[56] **LHCb** Collaboration, R. Aaij et al., *Observation of a resonance in $B^+ \to K^+ \mu^+ \mu^-$ decays at low recoil*, *Phys.Rev.Lett.* **111** (2013), no. 11 112003, [arXiv:1307.7595].

[57] A. Khodjamirian, T. Mannel, A. Pivovarov, and Y.-M. Wang, *Charm-loop effect in $B \to K^{(*)} \ell^+ \ell^-$ and $B \to K^* \gamma$*, *JHEP* **1009** (2010) 089, [arXiv:1006.4945].

[58] F. Muheim, Y. Xie, and R. Zwicky, *Exploiting the width difference in $B_s \to \phi\gamma$*, *Phys.Lett.* **B664** (2008) 174–179, [arXiv:0802.0876].

[59] S. Jger and J. Martin Camalich, *On $B \to V ll$ at small dilepton invariant mass, power corrections, and new physics*, *JHEP* **1305** (2013) 043, [arXiv:1212.2263].

[60] G. Hiller and R. Zwicky, *(A)symmetries of weak decays at and near the kinematic endpoint*, *JHEP* **1403** (2014) 042, [arXiv:1312.1923].

[61] **LHCb collaboration** Collaboration, R. Aaij et al., *Measurement of the $B^0 \to K^{*0} e^+ e^-$ branching fraction at low dilepton mass*, *JHEP* **1305** (2013) 159, [arXiv:1304.3035].

[62] **LHCb** Collaboration, R. Aaij et al., *Angular analysis of the $B^0 \to K^{*0}e^+e^-$ decay in the low-q^2 region*, arXiv:1501.0303.

[63] **LHCb** Collaboration, R. Aaij et al., *Measurement of the ratio of branching fractions $\mathcal{B}(B^0 \to K^{*0}\gamma)/\mathcal{B}(B^0_s \to \phi\gamma)$*, *Phys.Rev.* **D85** (2012) 112013, [arXiv:1202.6267].

[64] **LHCb** Collaboration, R. Aaij et al., *Differential branching fraction and angular analysis of the decay $B^0_s \to \phi\mu^+\mu^-$*, *JHEP* **1307** (2013) 084, [arXiv:1305.2168].

[65] *Precise Measurements of Exclusive $b \to s\mu^+\mu^-$ Decay Amplitudes Using the Full CDF Data Set*, .

[66] **BaBar Collaboration** Collaboration, P. del Amo Sanchez et al., *Study of $B \to \pi\ell\nu$ and $B \to \rho\ell\nu$ Decays and Determination of $|V_{ub}|$*, *Phys.Rev.* **D83** (2011) 032007, [arXiv:1005.3288].

[67] **Belle Collaboration** Collaboration, A. Sibidanov et al., *Study of Exclusive $B \to X_u\ell\nu$ Decays and Extraction of $\|V_{ub}\|$ using Full Reconstruction Tagging at the Belle Experiment*, *Phys.Rev.* **D88** (2013), no. 3 032005, [arXiv:1306.2781].

[68] **BaBar Collaboration** Collaboration, J. Lees et al., *Branching fraction measurement of $B^+ \to \omega\ell^+\nu$ decays*, *Phys.Rev.* **D87** (2013), no. 3 032004, [arXiv:1205.6245].

[69] **BaBar Collaboration** Collaboration, J. Lees et al., *Branching fraction and form-factor shape measurements of exclusive charmless semileptonic B decays, and determination of $|V_{ub}|$*, *Phys.Rev.* **D86** (2012) 092004, [arXiv:1208.1253].

[70] **CKMfitter Group** Collaboration, J. Charles et al., *CP violation and the CKM matrix: Assessing the impact of the asymmetric B factories*, *Eur.Phys.J.* **C41** (2005) 1–131, [hep-ph/0406184]. Updated results and plots available at: http://ckmfitter.in2p3.fr.

[71] **UTfit Collaboration** Collaboration, M. Bona et al., *The Unitarity Triangle Fit in the Standard Model and Hadronic Parameters from Lattice QCD: A Reappraisal after the Measurements of Δm_s and $BR(B \to \tau\nu_\tau)$*, *JHEP* **0610** (2006) 081, [hep-ph/0606167]. Updated results and plots available at: http://utfit.org/.

[72] P. Ball, V. M. Braun, Y. Koike, and K. Tanaka, *Higher twist distribution amplitudes of vector mesons in QCD: Formalism and twist - three distributions*, *Nucl.Phys.* **B529** (1998) 323–382, [hep-ph/9802299].

[73] G. Duplancic, A. Khodjamirian, T. Mannel, B. Melic, and N. Offen, *Light-cone sum rules for $B \to \pi$ form factors revisited*, *JHEP* **0804** (2008) 014, [arXiv:0801.1796].

[74] K. De Bruyn, R. Fleischer, R. Knegjens, P. Koppenburg, M. Merk, et al., *Branching Ratio Measurements of B_s Decays*, *Phys.Rev.* **D86** (2012) 014027, [arXiv:1204.1735].

[75] S. Descotes-Genon and J. Virto, *Time dependence in $B \to V\ell\ell$ decays*, arXiv:1502.0550.